

國立交通大學

電子物理系光電物理組

碩士論文

氧化鋅摻鉻薄膜的磁性研究

The study on the ferromagnetism in
Cr-doped ZnO films

The logo is a circular emblem with a blue border. Inside the circle, there are stylized representations of books and a gear, with the letters 'E', 'S', and 'A' arranged vertically. Below the gear, the year '1956' is visible.

研究生：李秉翰

指導教授：莊振益 教授

中華民國九十六年七月

誌謝

兩年的碩士研究生活結束了，真的要感謝很多人。首先要感謝莊老師對我的指導，與老師的討論總是讓我獲益良多，常常在我研究陷入瓶頸時給予方向與建議。還有很感謝林老師、溫老師、吳老師跟羅老師，除了提供我很多實驗上的想法之外，從老師們身上我也學到了很多做研究的態度與方法。也很感謝旭禎學長、燦耀學長及家鑑學長，在我剛進實驗室時給予指導。麻煩最多的是昌學長跟維仁學長，總是提供我很多量測以及儀器上的經驗。還有很感謝常常陪我討論的簡博、訓全、宗漢及家宏學長，雖然嘴砲的時間還是比較多。實驗室的同學們：右儒、竣揚、裕閔、阿福、阿江、明道、東煌、雅鈴、大捲，恭喜我們終於可以迎接不用鍍膜的日子了，雖然解釋數據還是很令人頭痛。嘉恬、珈芸、書宏、宗祐、仕豪、彥宇、邵瑛、怡君、家治，跟你們相處的日子很有趣，還有，要吃好料的記得要找我喔。還有給給、AK、黑鬼、BOBO、幹宏，你們的不定時出現點綴了我的生活。最後要感謝我的父母及家人，在這一路上他們給予我的支持是不可衡量的。還有香吟，遇到妳是我這輩子最快樂的事情，有妳的陪伴，我才得以在壓力下喘一口氣。最後要說的是，我很開心是在這個實驗室完成我的碩士學位，這裡的人與氣氛都很棒，讓我度過了很充實的兩年，也會是很好的一段回憶。

Table of Contents

(1) Abstract	1
(2) Chap. 1 Introduction	2
(3) Chap. 2 Theory of ferromagnetism in oxides and related phenomenon	9
2.1. Classification of various kinds of magnetism	9
2.1.1 Diamagnetism	9
2.1.2 Paramagnetism	10
2.1.3 Ferromagnetism	11
2.1.4 Antiferromagnetism	13
2.1.5 Spin-glass	13
2.1.6 Superparamagnetic	14
2.2. The bound magnetic polaron (BMP) model	15
(4) Chap. 3 Experiments	18
3.1. Sample Preparation	18
3.1.1 Target Fabrication	18
3.1.2 Pulse Laser Deposition (PLD)	18
3.2. Measurements	21
3.2.1 X-ray Diffraction (XRD)	21
3.2.2 Super-conducting quantum interference device (SQUID)	23
3.2.3 Resistivity measurements	25
(5) Chap. 4 Results and discussions	28
4.1. Influence of various growth conditions on FM in 1% Cr-doped ZnO	28
4.2. Phase transition from ferromagnetic spin-glass to ferromagnetic insulator	40
(6) Chap. 5 Summary and Conclusions	42
(7) References	44



Abstract

In the field of dilute magnetic semiconductors (DMS), Mn and Co were the most popular dopants in ZnO host, and the two systems were widely studied over the past two decades. Several models were proposed to explain the magnetic behaviors in DMS, but the origin of the ferromagnetism is still a matter of debate. The seemingly contradictory results obtained by Hong *et al.* [19] and Roberts *et al.* [17] suggest an alternative way of resolving this problem by exploring the magnetic behavior in the system of Cr-doped ZnO. The relation between the magnetic behavior and the growth conditions was discussed in detail in this work. It is believed that the induced FM is much affected by the oxygen vacancies in this system. Raising the concentration of oxygen vacancies might induce the FM in this system. Phase transition is also observed as the doped Cr increased from 1% to 5%. The crystalline structure was checked by X-ray diffraction (XRD), and the magnetic behavior was measured by super-conducting quantum interference device (SQUID). The magnetic behavior can be explained by Coey's [12] theoretical prediction based on bound magnetic polaron model.

Chapter 1

Introduction

Nowadays, most of the technological applications in electronics are based on manipulating the electronic charge. Over the last half century, in order to pursue higher and higher device performance, reducing the feature size has been the major driving force leading to today's high-tech semiconductor industry. However, this seemingly extremely successful methodology is facing apparently insurmountable obstacles. For instance, as the gate oxide gets to a few atomic layers thick, the leakage current straying through it has become an issue. On the other hand, when the feature size of devices gets down to nanometer scale, quantum size effects may change the device function in a totally unexpected way. Both, unfortunately, are inherent to either the intrinsic properties of the materials or the fundamental physics, and, hence, may not be solvable in "conventional" manners. As a result, instead of trying to tackle all the problems by pushing the technologies to their limits, recently, scientists have been sketching out a family of novel devices based on the revolutionary ideas called "spintroincs". The core concept of this new field is trying to utilize the second property of electrons (or holes), the "spin", for carrying, manipulating, and storing information.

The spin-based devices, such as spin-FET, spin-LED, and even the quantum bits for quantum computation promise the potential advantages of nonvolatility, faster data processing speed, lower electric power

consumption, and higher integration densities compared to conventional semiconductor devices [1]. However, before the real applications of these devices, several outstanding issues must be resolved. For instance, one must find a way to transport the spin-polarized currents efficiently, to control and to manipulate the spin polarization, preferable at room temperature [1]. For these purposes, the so called dilute magnetic semiconductors (DMS) have been developed. The most important characteristic that the DMS should have is to exhibit a Curie temperature (T_c) above room temperature such that the material can exhibit ferromagnetism (FM) and perform all the function conveniently. In fact, this issue has been a major bottleneck in the early researches, and the practical utilization of DMS was once believed to be extremely unlikely if not impossible. However, Dietl's work based on Zener model [2] and Ruderman-Kittel-Kasuya-Yoshida (RKKY) interaction revived attention and interests among scientists again because of the precise theoretical calculation not only confirmed the T_c of $\text{Ga}_{1-x}\text{Mn}_x\text{As}$ and $\text{Zn}_{1-x}\text{Mn}_x\text{Te}$ but also gave further predictions for searching DMS with higher T_c [3]. The results are reproduced and displayed in Fig. 1.1.

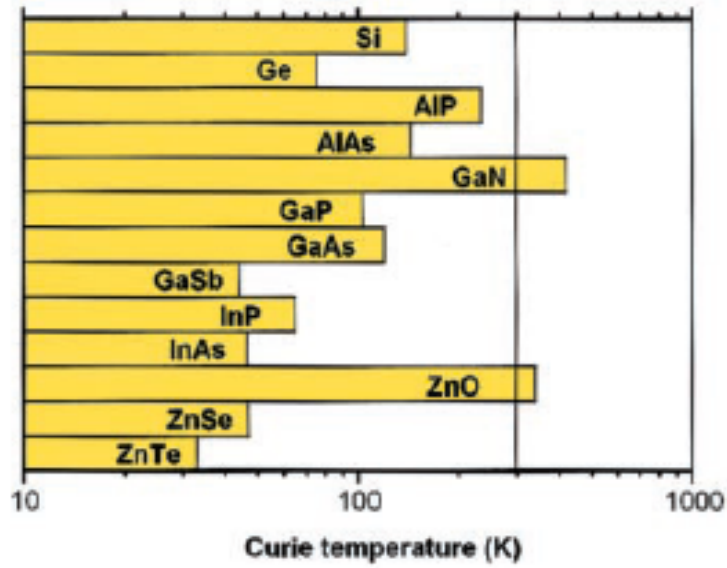


Fig.1.1
 Computed values of the Curie temperature T_C for various p -type semiconductors containing 5% of Mn and 3.5×10^{20} holes per cm^3 [3]

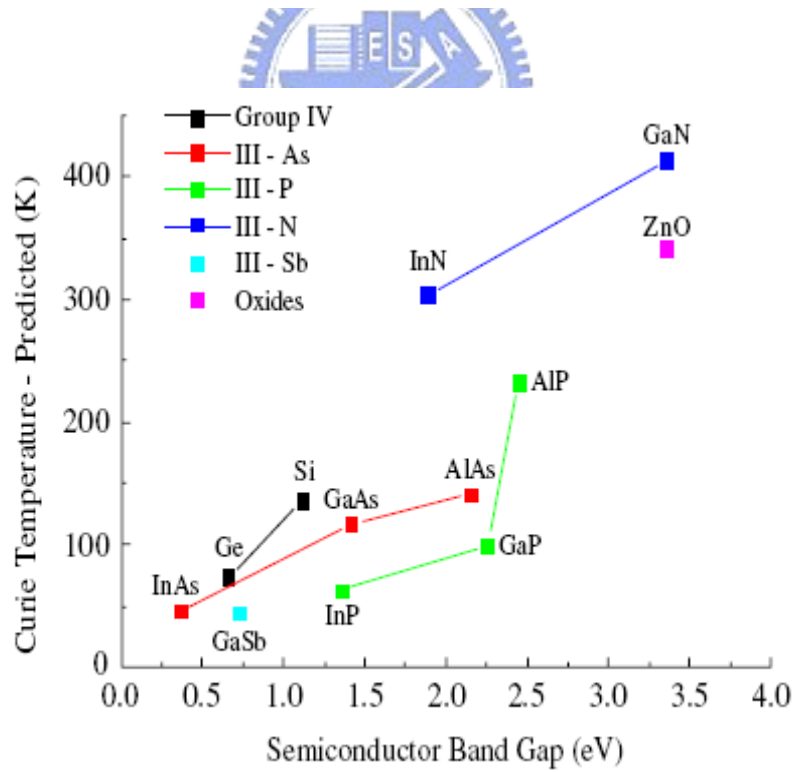


Fig.1.2
 Predicted Curie temperatures in oxides and semiconductors [5].

According to Dietl's mean-field Zener model, the coupling between the holes and the spins of localized magnetic cations, obtained by doping transition metals, would be stronger in wide-bandgap materials due to its short bond length [4]. The correlations between T_C and magnitude of band gap of the host semiconductors are displayed in Fig. 1.2 [5]. Among various *p*-type semiconductors containing 5% of Mn and 3.5×10^{20} holes per cm^3 , ZnO and GaN are the most promising candidates with FM above room temperature according to Dietl's prediction. It is also the reason that most of the recent researches have been focused on these two materials.

So far there are lots of observations reporting FM above room temperature in various host materials, like ZnO [6], GaN [7], SnO_2 [8], and TiO_2 [9], but the mechanism of FM in doped oxide materials is still in extensive debate. Besides Dietl's model, several models have been proposed, such as double exchange [10], F-center exchange [11], and the bound magnetic polaron (BMP) model [12]. It is also noted that the possibility of the ferromagnetic cluster still can not be completely ruled out in interpreting the observed FM characteristics in various DMS materials [13,14,15].

In addition to Dietl's prediction [3], Sato and Katayama-Yoshida [16] theoretically investigated the FM in transition-metal-doped ZnO by *ab initio* calculations based on the local density approximation. Their results agree with Dietl's notion that ferromagnetic ordering of Mn is favored when mediated by mobile holes. They also investigated the FM in

other transition- metal-doped ZnO. Unlike the case in Mn-doped ZnO, the ferromagnetic ordering was predicted to occur without the need of additional charge carriers for V, Cr, Fe, Co, and Ni –doped ZnO (as shown in Fig.1.3).

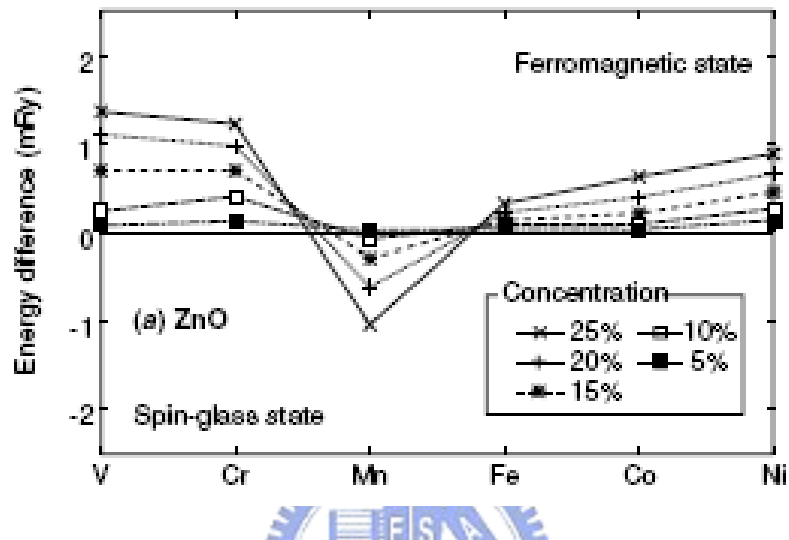


Fig.1.3

Stability of the ferromagnetic states in ZnO-based DMS. The vertical axis is the energy difference between the ferromagnetic state and the spin-glass state. A positive energy difference indicates the ferromagnetic is more stable than the spin-glass state.

In Fig.1.3, it is evident that the ferromagnetic state is more energetically favorable in Cr-doped ZnO than that in Mn or Co-doped ZnO. Besides, Cr is favorable for doping because the radii of Cr^{2+} (0.073 nm) is close to the radii of Zn^{2+} (0.074 nm), and Cr^{2+} ($4 \mu_B$) has larger moment [17]. However, early studies on Cr-doped ZnO film showed no FM [18]. In 2003, Satoh *et al.* [19] claimed to observe FM in their 20% Cr-doped films at room temperature. They also measured the optical and magnetic properties, although little information about their films was revealed. In

2005, Robert [17] and Hong [20] observed the evidence of FM in Cr-doped ZnO, respectively. The growth conditions of their films are listed in the table 1.1. However, very different results were reported after the samples were annealed. Roberts *et al.* observed enhanced FM in the sample with stronger XRD peak intensity after the films were post-annealed in ultra high vacuum at 600°C. On the contrary, Hong *et al.* [20] observed diminishingly small FM signals in their samples postannealed in 760 torr of oxygen atmosphere at 500 °C for 12 hours, despite that stronger XRD peak intensity was obtained. Hong *et al.* claimed that the role of defect induces the FM in Cr-doped ZnO because they observed very different lattice parameters of ferromagnetic samples ($a=2.95 \text{ \AA}$, $c=3.91 \text{ \AA}$; $a=2.96 \text{ \AA}$, $c=3.91 \text{ \AA}$, or $a=2.65 \text{ \AA}$, $c=5.14 \text{ \AA}$) from the undoped ZnO ($a=3.467 \text{ \AA}$, $c=5.129 \text{ \AA}$). They assume that, in this type of compound, perfect crystallinity doesn't go along with FM. Moreover, they believe that filling up oxygen vacancies does not enhance the FM at all. In their study, FM in Cr-doped ZnO films were obtained with two sets of very different growth conditions. In order to elucidate the underlying mechanisms leading to the discrepancies observed in the literature, we examined the growth conditions in detail, like the substrate temperature, the pressure of oxygen atmosphere, and the cooling conditions, to understand which parameter dominates the FM in Cr-doped ZnO.

In this study, we focus on the magnetic behavior in 1 at. % and 5 at. % Cr-doped ZnO films under various growth conditions. These results would be discussed in the chapter 4.

Table 4.1

Comparison between the work of Roberts *et al.* [17] and that of Hong *et al.* [20]

Author	Bradley K.Roberts	Nguyen Hoa Hong
Method	RF magnetic sputter	PLD
Substrate	α - Al ₂ O ₃ (1-102)	α - Al ₂ O ₃ (1-102)
Concentration	Cr : 9.5% (> 9.5% => poly or amorphous)	Cr : 5%
Condition	250~550±50 °C (480°C is optimal) Ar:5x10 ⁻³ torr	1.650 °C, P _{O2} :10 ⁻¹ Torr, cooled in 0.3torr 2.400 °C, P _{O2} :10 ⁻⁶ Torr, cooled in 0.02torr
Speed	<0.3 Å/s (<i>otherwise poly or amorphous</i>)	λ =248 nm,10 Hz,1.8 J/cm ²
Thickness	500~700 Å	2000 Å
Annealing	Some are annealed at 10 ⁻⁹ Torr and 600 °C	Some are postannealed at 760 Torr and 500 °C for 12h
Notation	Insulator at 9.5%; T _C >365 K;	Down slope in <i>M-H</i> curve is related to residual contribution of the substrate ; T _C >300 K.

Chapter 2

Theory of ferromagnetism in oxides and related phenomena

2.1 Classification of various kinds of magnetism

Magnetism is an intrinsic manifestation of quantum mechanics. For a free atom, the magnetic moment has three principal sources: the spin with which electrons inside the atom are endowed; their orbital angular momentum about the nucleus; and the change in the orbital moment induced by an applied magnetic field [21]. Macroscopically, the magnetism is often classified by the ratio between the magnitude of magnetization (M) in the material induced by the externally applied field to that of the applied magnetic field (H), i.e. by the magnetic susceptibility (χ), defined by the following equation :

$$\chi = M/H \quad (\text{CGS}) \quad \text{or} \quad \chi = \mu_0 M/H \quad (\text{SI})$$

In both unit systems χ is dimensionless. Depending on the magnitude, various kinds of magnetism are classified as follows.

2.1.1 Diamagnetism (DM)

Diamagnetism is associated with the tendency of electrical charge to resist the change in the interior of an atom (or a matter) induced by the applied magnetic field. The magnetization is weak and antiparallel to the external field. It appeared only when an external magnetic field is applied. Consequently, the susceptibility is negative and the value is

on the order of 10^{-5} per unit volume in SI unit.

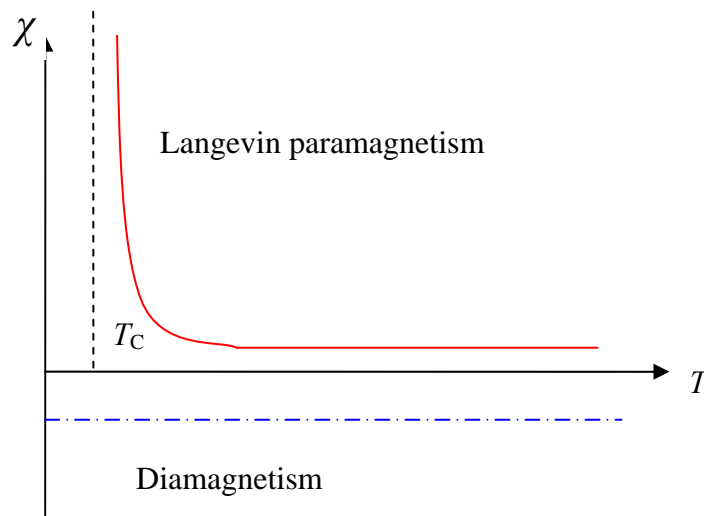


Fig. 2.1

Characteristic magnetic susceptibilities of diamagnetic and paramagnetic substance.



2.1.2 Paramagnetism (PM)

For some solid materials, each atom has net magnetic dipole moment from the spin of electrons or their orbital angular momentum. The direction of the magnetic dipole moment of each atom is random so that there is no net macroscopic magnetization in zero applied magnetic field. While a magnetic field is applied, the magnetic dipole moments tend to align along the direction of magnetic field so that a positive magnetization can be observed. The relation between temperature and susceptibility of most paramagnets obeys the Curie-Weiss law as follows :

$$\frac{M}{B} = \frac{C}{T-T_c} ,$$

where C is known as the Curie constant, and T_C is known as the Curie temperature. Above T_C , the spontaneous magnetization vanishes.

2.1.3 Ferromagnetism (FM)

Ferromagnetism is a critical phenomenon, involving a phase transition that occurs at a critical temperature, i.e. T_C . Above T_C , such material behaves like paramagnets; below T_C , it has spontaneous magnetization even with no applied magnetic field because the magnetic moments tend to align in the same direction via exchange interaction. If the applied magnetic field is strong enough, ferromagnets will attain to its saturation magnetization. When the magnetic field is reduced from the saturation field to zero, the magnetization will not back to zero. This hysteresis phenomenon is one of the typical characteristic of ferromagnetism.

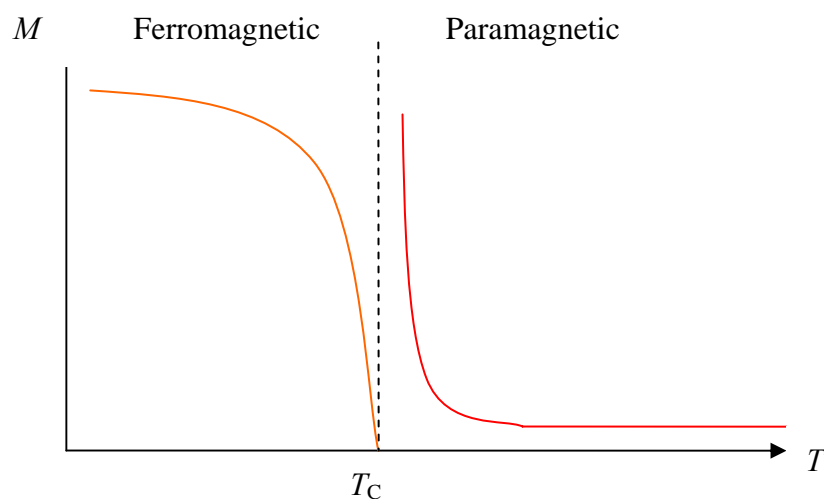


Fig. 2.2

Characteristic magnetic susceptibilities of ferromagnetic. Above T_C , the ferromagnetic substance would be paramagnetic.

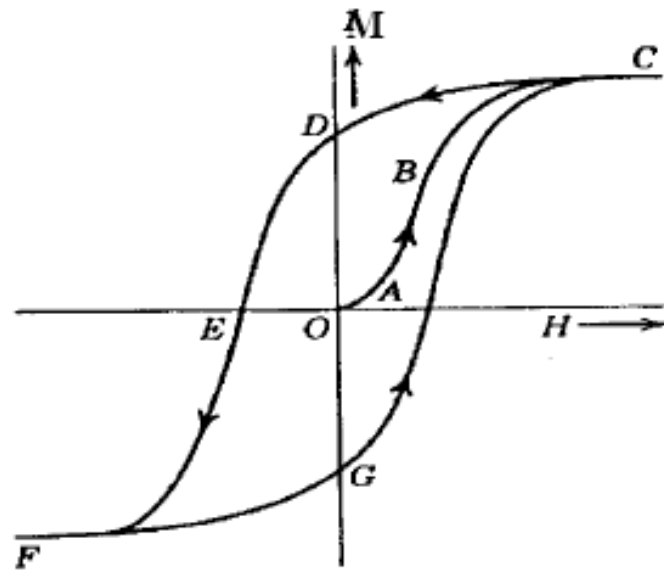


Fig. 2.3
Hysteresis curve for typical ferromagnetic substance.

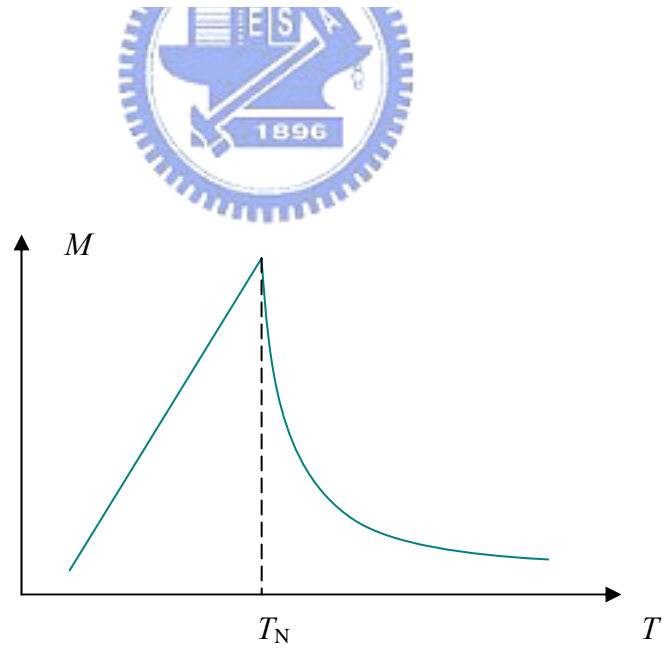


Fig. 2.4
Characteristic magnetic susceptibilities of antiferromagnetic substance.

2.1.4 Antiferromagnetism (Anti-FM)

In antiferromagnets, the magnetic moment antiparallels to its nearest neighbor below the Neel temperature. As the temperature is increased, the coupling between magnetic moments becomes weaker so that the susceptibility becomes larger. Above Neel temperature, the magnetic moments would be randomly aligned, and the antiferromagnet behaves like paramagnet.

2.1.5 Spin-glass (SG)

Spin-glass is one of the more complicated forms of magnetism. Provided that the magnet moments are randomly distributed, if the spin can't satisfy the coupling between itself and its second-neighbor bonds, the spin will be "frustrated". Such situation is the origin of spin-glass. In materials, structure disorder and disrupted interaction originated from impurity doping can all act to frustrate the coupling and lead to SG state.

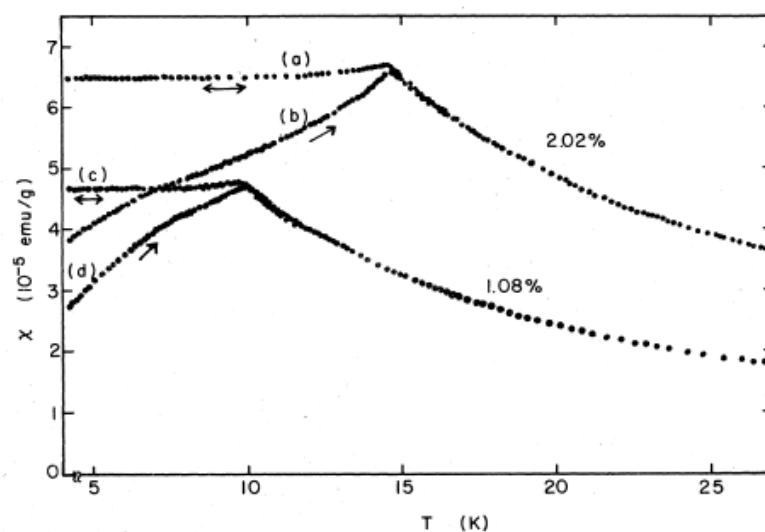


Fig. 2.5

Typical $M-T$ curves of CuMn (1 and 2 at. %), spin-glass substance, under field cooled [(a), (c)] and zero-field cooled [(b), (d)] protocols [22].

2.1.6 Superparamagnetic (SPM)

When the size of the ferromagnetic particles is reduced below the single domain limit (~15 to 20 nm for iron oxide), they exhibit superparamagnetism at room temperature followed by a spin-glass like transition at low temperature [23]. An operational definition of SPM would include at least two requirements. First, the magnetization must show no hysteresis, since that is not a thermal equilibrium property. Second, except for particle interaction effects, the magnetization curve for an isotropic sample must be temperature dependent to the extent that curves taken at different temperature must approximately superimpose when plotted against H/T after correction for the temperature dependence of the spontaneous magnetization [24], as shown in Fig. 2.6.

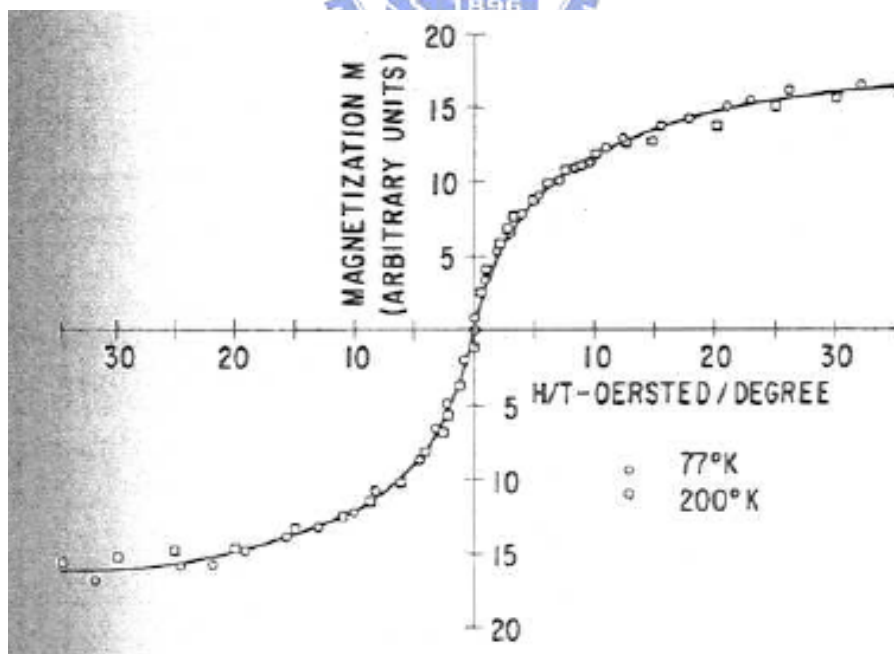


Fig. 2.6

H/T superposition of these magnetization curves of 22 Å radius iron particles in mercury [24].

2.2 The bound magnetic polaron (BMP) model

The BMP model has been widely used to explain the FM in insulators or in semiconductors. The exceptionally large ordered moments per transition-metal cation at low concentrations are unprecedented, exceeding those in almost all known oxides or alloys, including the pure metal [25]. Conventional superexchange or double-exchange interactions can not produce long-range magnetic order at concentrations of magnetic cations of a few percent. In 2005, Coey *et al.* [12] proposed that ferromagnetic exchange in some kinds of materials can be mediated by shallow donor electrons that form bound magnetic polarons. When the BMPs start to overlap, a spin-split impurity band is created. The idea can be understood by the schematic illustration shown in Fig. 2.7.

In Fig. 2.7, the donors from oxygen vacancies tend to form bound magnetic polarons, coupling the moments of $3d$ cations within their orbits. The moments of $3d$ cations coupling with the same donors would parallel to each other so that the effective coupling is ferromagnetic. As the density of defects increases, the hydrogenic orbits associated with the randomly positioned defects overlap, and the donor impurity band forms. There might be a change from insulator-like to metal-like on account of the increase of defects. Below the cation percolation threshold, as the doped concentration of $3d$ elements increases, the antiferromagnetic super-exchange can not create long-range order; at most it will act within small groups of nearest-neighbor cations, which reduce the average moment per

cation. If the concentration goes beyond the percolation limit, there will be a phase transition from ferromagnetic state to antiferromagnetic state. The phase diagram that Coey *et al.* proposed is reproduced in Fig. 2.8. Our study focused on the doped concentration from 1% to 5 %, and we observed a phase transition from ferromagnetic spin-glass to ferromagnetic insulator.

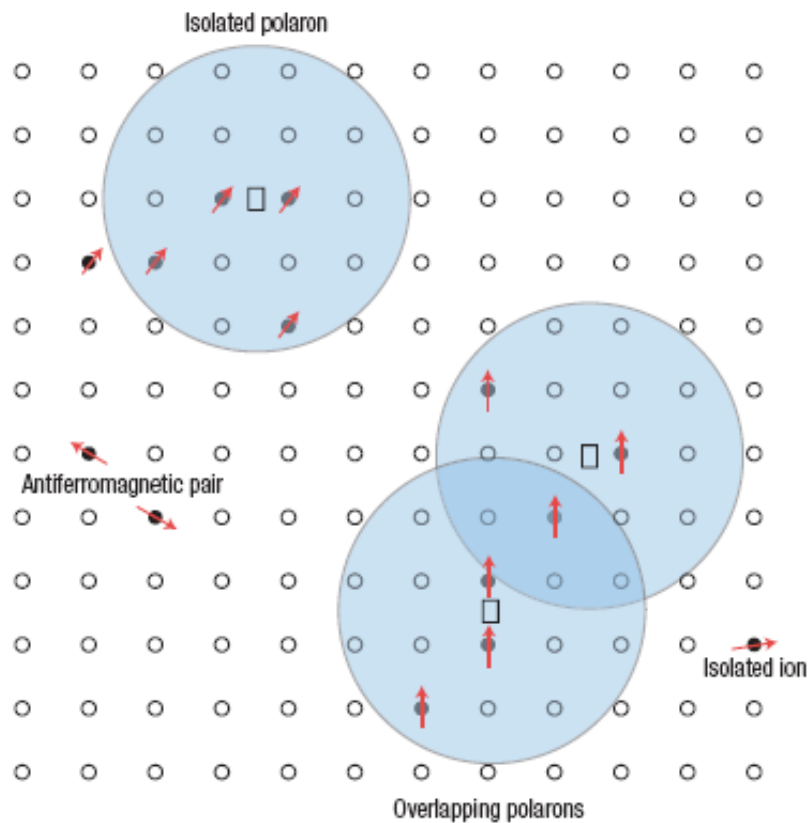


Fig. 2.7

A donor electron in its hydrogenic orbit couples with its spin antiparallel to impurities with a $3d$ shell that is half-full or more than half-full. Cation sites are represented by small circles. Oxygen is not shown; the unoccupied oxygen sites are represented by squares. [12]

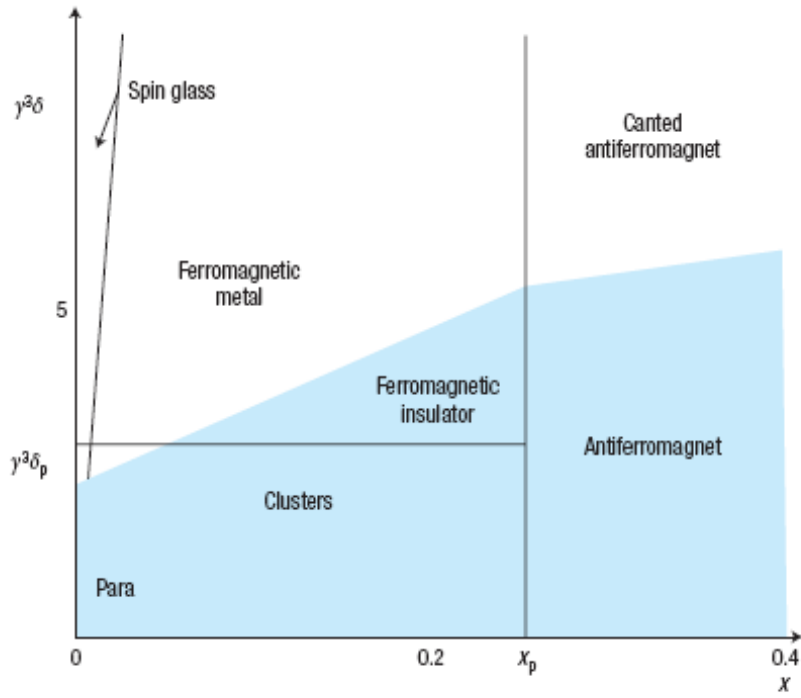


Fig. 2.8

The magnetic phase diagram for dilute ferromagnetic semiconductors. The electrons are localized in the shaded area. x_p and δ_p are the cation and donor polaron percolation thresholds, respectively. γ is the ratio of the radius of the hydrogenic donor orbital to the Bohr radius. [12]

Chapter 3

Experiments

3.1 Sample Preparation

3.1.1 Target Fabrication

The targets used for fabricating the pure $\text{Zn}_{0.99}\text{Cr}_{0.01}\text{O}$ and $\text{Zn}_{0.95}\text{Cr}_{0.05}\text{O}$ films were synthesized by applying the standard solid-state route. Take $\text{Zn}_{0.99}\text{Cr}_{0.01}\text{O}$ for example, we mixed ZnO and Cr_2O_3 powders together with proportions of aimed stoichiometry - ZnO(10.8972 g) and Cr_2O_3 (0.1028 g). The mixture was ground and heated at 1100 °C for 12 hours to promote the reactions among constituents. After repeating the above procedures 3 times, the solidified mixture was grounded again and then pressed in the mold to form the target body. The target body was heated again at 1100 °C for 24 hours and cooled in ambient conditions temperature.

3.1.2 Pulse Laser Deposition (PLD)

The basic concept of PLD is to ablate materials from the target and deposit the ablated materials onto the substrate by using photons with high energy. Samples discussed in this study were all deposited by the KrF excimer laser with an energy of 350 mJ and a repetition rate of 5 Hz. The greatest virtue of PLD is that the stoichiometry of the target can be preserved in the obtained films due to the explosive ablation resulted from the extremely high heating rate of the target surface due to

pulsed-laser irradiation. This process in turn leads to the congruent evaporation of the target irrespective of the vaporization temperature of the individual constituent element or compound contained in the target. Therefore the doping concentration can be controlled by changing the composition of target. The quality of films can also be influenced by factors such as the oxygen pressure during growth, the temperature of the substrate, and the energy and repetition rate of the laser beam. The influence of these factors on the FM of Cr-doped ZnO films would be discussed in detail in chapter 4. We chose the *R*-cut sapphire ((1-102) -Al₂O₃) as the substrate for growing ZnO films because its lattice mismatch with ZnO is smaller than that of *C*-cut sapphire ((0001) -Al₂O₃), although both have been widely used in the study of transition-metal-doped ZnO.

A simple schematic diagram of the PLD system is shown in Fig. 3.1, and the detailed procedures for preparing the ZnO films are described below :

1. Clean the substrate in acetone, methanol, and DI water, respectively, under ultrasonic vibration for 15 minutes.
2. Repeat above processes for 3 times.
3. Attach the substrate on the stainless steel plate by silver paste.
4. Heat the plate at ~100 °C till the silver paste is solidified.
5. Clean the surface of substrate by nitrogen gas.
6. Put the plate in the chamber of PLD system.
7. Pump the chamber till the base pressure is lower than 10⁻⁶ Torr for 1 hour at least.
8. Heat the substrate to the preset temperature.

9. Aerate the chamber with oxygen to the expected pressure.
10. Set the power, repetition rate and counts of excimer pulse laser.
11. Start to deposit the film on the substrate.
12. Cool the chamber under required conditions.
13. Take out the sample.

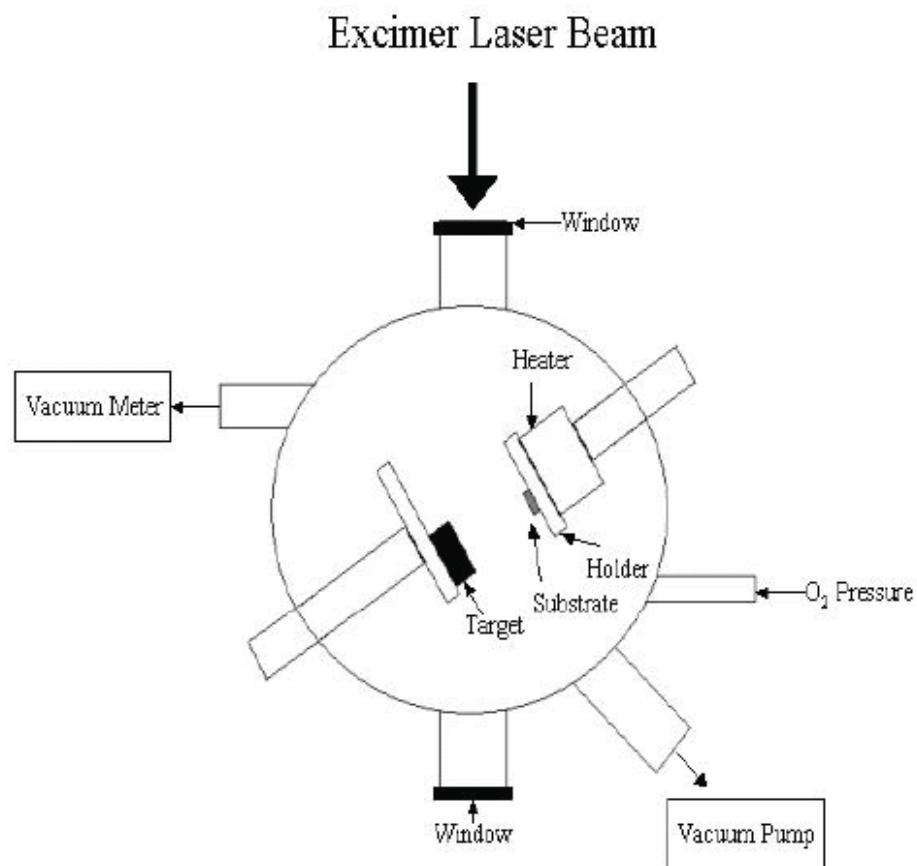


Fig.3.1
The configuration of PLD system.

3.2 Measurements

3.2.1 X-ray diffraction (XRD)

The crystal structure of all samples were checked by X-ray diffraction (XRD) measurements. Briefly, XRD is based on Bragg diffraction condition :

$$2d \cdot \sin \theta = n\lambda$$

where d is the distance between successive parallel planes, θ is the angle between incident X-ray and the normal of the lattice plane, n is an integer, and λ is the wavelength of the X-ray. XRD can also be taken as a tool for the initial analysis of composition. The simple schematic illustration of XRD is shown in Fig. 3.2.

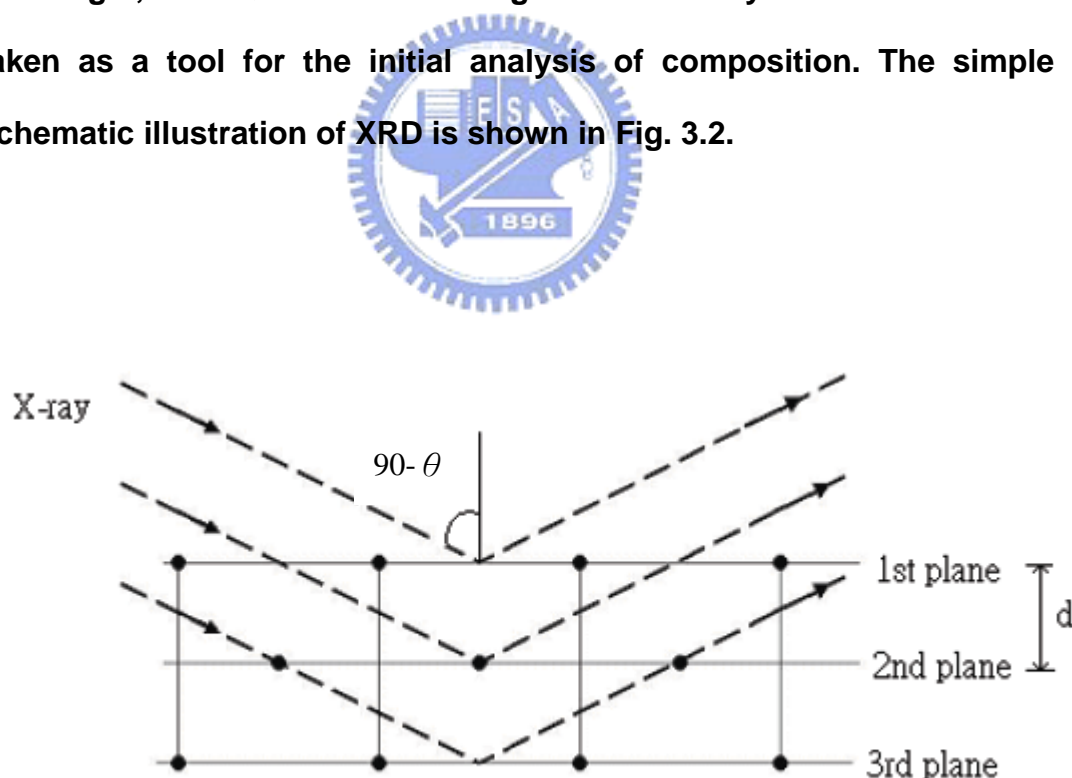


Fig.3.2

The schematic illustration of the derivation of Bragg diffraction condition used in XRD analyses.

In order to reduce the possible secondary phases in our films, a pure target should be helpful. In other words, it would be ideal if the Zn ions can be substituted by the Cr ions perfectly. Unfortunately, the targets synthesized by the standard solid-state reaction route were found to consist of two compounds : ZnO and ZnCr₂O₄. The XRD patterns of the 1% and 5% Cr- doped ZnO targets are shown in Fig. 3.3. However, as will be demonstrated later, despite of the non-ideal targets, pure and highly crystallographic oriented Cr-doped-ZnO films can still be obtained. As shown in Fig. 3.4., c-axis oriented ZnO and Cr-doped ZnO films were evidently obtained by the present deposition process.

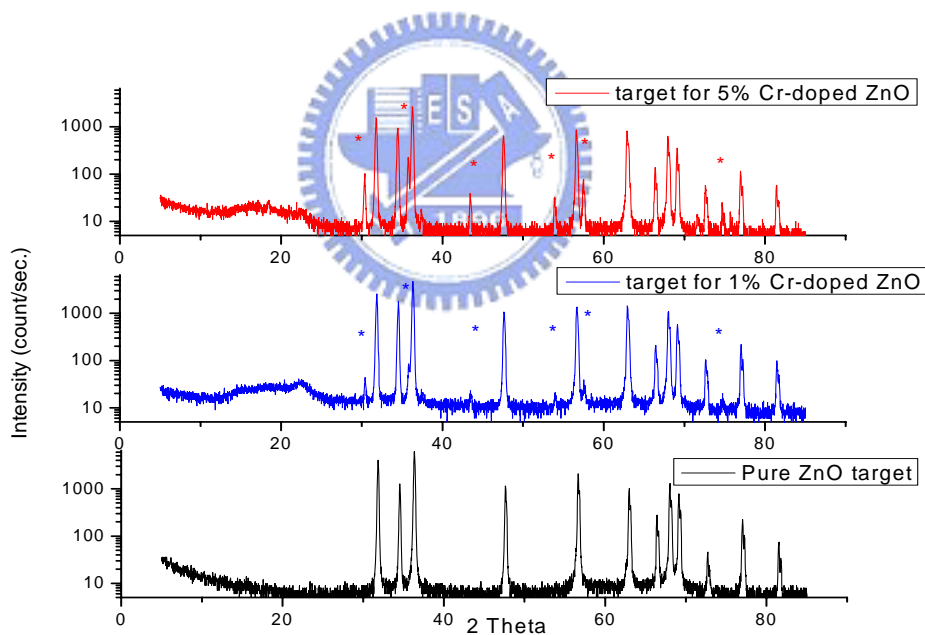


Fig.3.3

XRD patterns of targets with different doping concentrations.

The mark “*” represents the peaks of ZnCr₂O₄. Others are the peaks of ZnO.

It shows that there are mixed phases in the targets. The XRD of the pure ZnO target is also displayed for comparison.

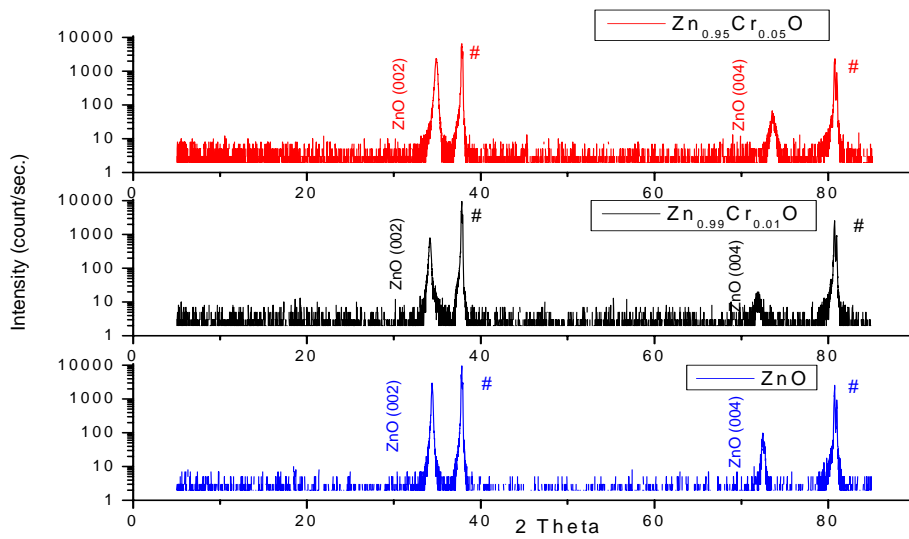


Fig.3.4

XRD patterns of different Cr-doped concentrations films grown with the same conditions. Samples were grown in an oxygen atmosphere of 10^{-4} Torr and then cooled rapidly under P_{O_2} over 760 Torr to room temperature.

The mark “#” represents the peaks of *R*-cut sapphire. The absence of secondary phase was evidenced by XRD results.

3.2.2 Super-conducting quantum interference device (SQUID)

SQUID is a delicate equipment integrated with electronic, mechanical, low-temperature, and vacuum technique. It is also the most sensitive and powerful apparatus for measuring the magnetic properties of materials so far. The SQUID we used is provided by the NCTU Instrument Center. In this study, both the 1% and 5% Cr-doped films exhibit FM when prepared under certain growth conditions. The results for 1% Cr-doped ZnO films (ZCO1) are shown in Fig. 3.5 and Fig. 3.6. It is evident that there is a remanent magnetization below 350 K in the sample. In Fig. 3.6, *M-H* curve shows small hysteresis which is one of the characteristics of FM. Furthermore, the hard axis and easy axis behaviors were also observed in *M-H* curve. The underlying physics gives rise to these phenomena will be discussed later in chapter 4.

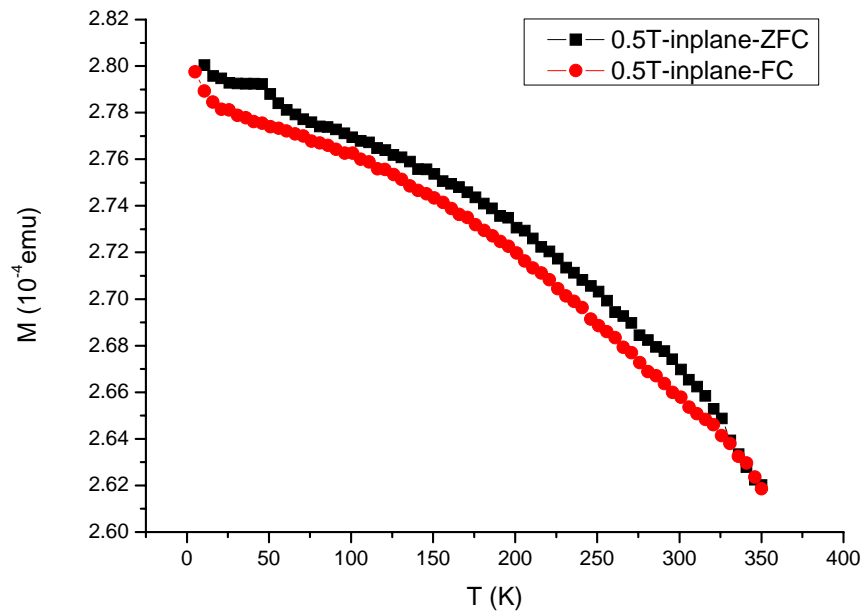


Fig. 3.5

M - T curves for ZCO1 films fabricated in P_{O_2} of 10^{-4} Torr at $500\text{ }^{\circ}\text{C}$ and then cooled rapidly to RT.

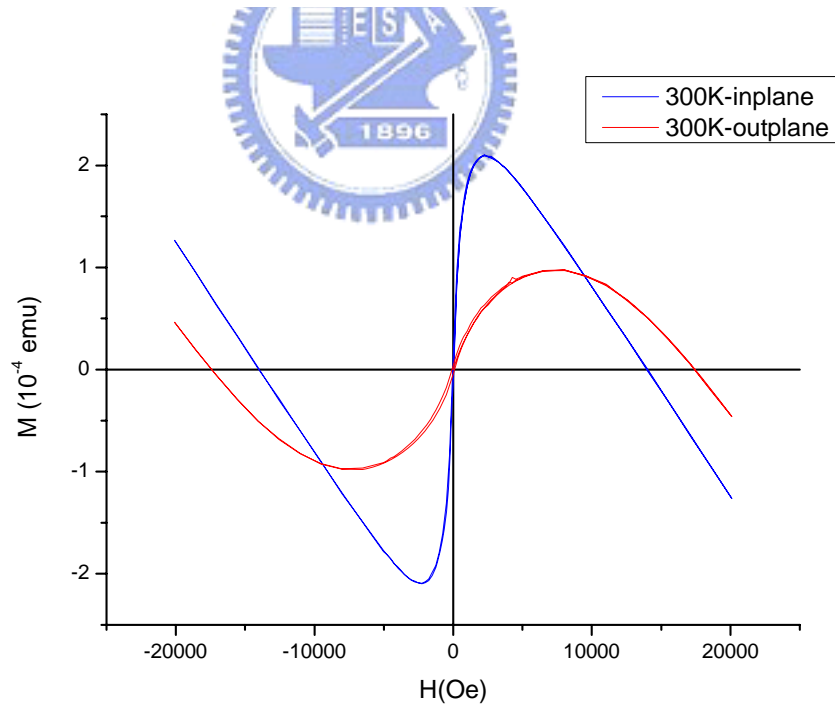
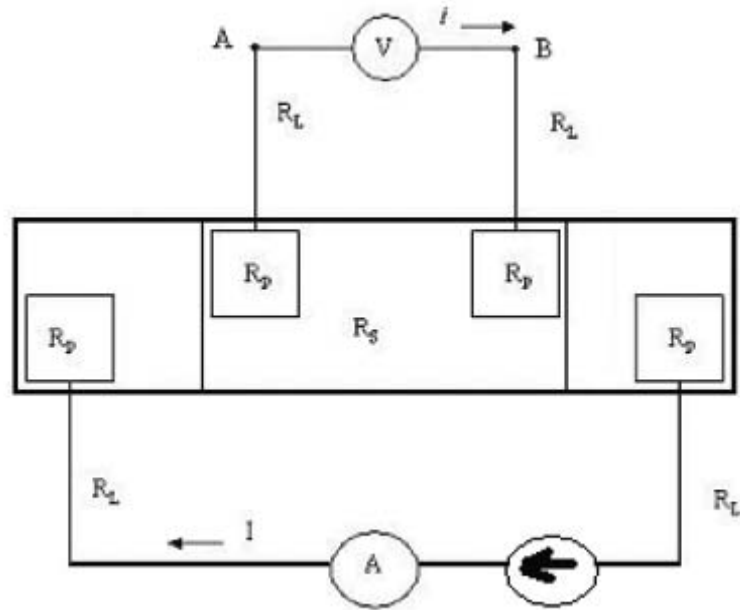


Fig. 3.6

M - H curves for ZCO1 films fabricated in P_{O_2} of 10^{-4} Torr at $500\text{ }^{\circ}\text{C}$ and then cooled rapidly to RT. This curve is uncorrected, i.e. the diamagnetic contribution of the substrate has not been subtracted.

3.2.3 Resistivity measurements

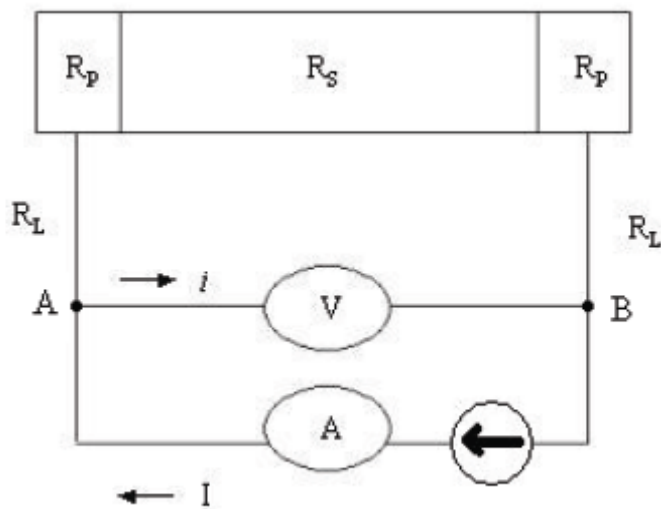
The standard four-probe configuration (Fig. 3.7) is employed to measure the resistance of samples. Unlike the traditional two-probe configuration (Fig. 3.8), four-probe configuration method can avoid the combined voltage-drop including pad resistance and line resistance by separating the current-source pads and the voltage-meter pads. In other words, the resistance can be measured exactly by the standard four-probe configuration method. Comparing Equation (3-1) and (3-2), the voltage contribution of pad resistance could be neglected by four-probe configuration method. In addition, the van der Pauw method [26] was also utilized in the resistivity measurement. The noted virtue of the van der Pauw method is that it can be applied on the sample with arbitrary shape. In order to obtain more accurate results, the dc voltage between different contacts was measured, and sample geometry we chose was shown in Fig. 3.9(b). The accurate process is referred to the method proposed by NIST (National Institute of Standard and Technology) [27].



$$R_M = \frac{V_{AB}}{I} = \frac{(I-i) \times R_s + i \times (2R_L + 2R_p)}{I}$$

$$\because i \approx 0 \Rightarrow I-i \approx I \Rightarrow R_M = \frac{I \times R_s + 0}{I} = R_s \quad \text{Eq. (3-1)}$$

Fig. 3.7
The configuration of four-probe resistance measurement system



$$R_M = \frac{V_{AB}}{I} = \frac{(I-i) \times (R_s + 2R_L + 2R_p)}{I}$$

$$\because i \approx 0 \Rightarrow I-i \approx I$$

$$\Rightarrow R_M = R_s + 2R_L + 2R_p$$

Eq. (3-2)

Fig. 3.8
The configuration of two-probe resistance measurement system

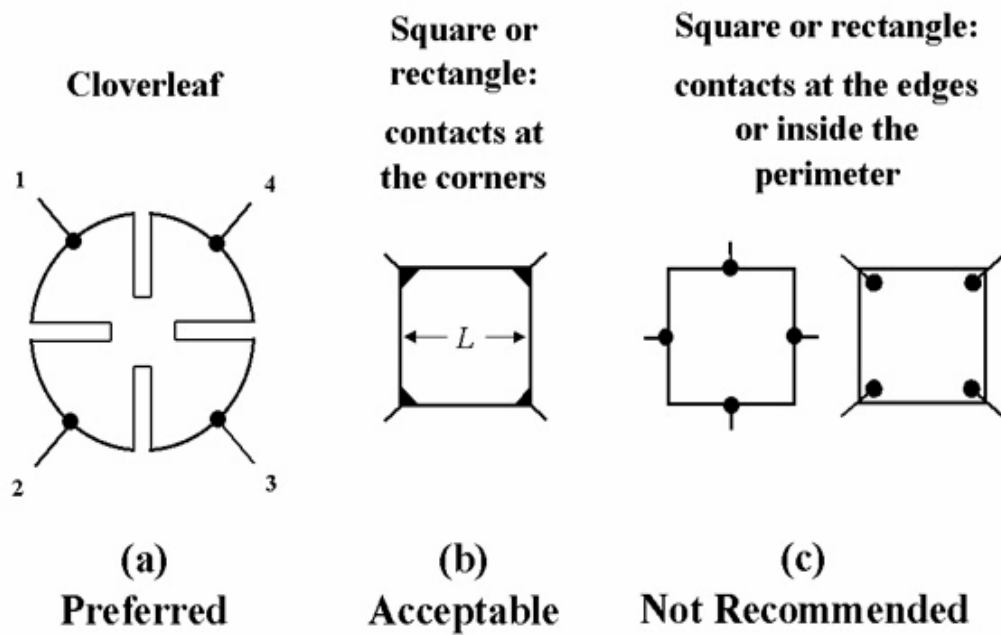


Fig.3.9

Sample geometries for van der Pauw resistivity and Hall effect measurements. The cloverleaf design will have the lowest error due to its smaller effective contact size, but it is more difficult to fabricate than a square or rectangle. [27]



Chapter 4

Results and discussion

4.1 Influence of various growth conditions on FM in 1% Cr-doped ZnO

Hong *et al.* [19] observed FM in 5% Cr-doped ZnO films fabricated on *R*-cut sapphire (ZCO5R) with two very different growth conditions. These conditions were listed in table 4.1. The fact that FM can be obtained in Cr-doped ZnO over such a wide range of growth temperature and oxygen environment implies FM is rather insensitive to growth conditions, which is in sharp contrast to other results. In this chapter, we perform systematic studies by treating each growth parameter separately. We fixed all other parameters while varied one particular parameter over a rather wide range and studied the effects of each parameter on the film transport and magnetic properties. Both 1% Cr-doping and 5% Cr-doping samples were investigated and compared.

Table 4.1 Growth conditions of Hong's ferromagnetic ZCO5R films [20]

	Substrate temperature	P_{O_2} during growth	P_{O_2} during cooling
Sample 1	650 °C	10^{-1} Torr	0.3 Torr
Sample 2	400 °C	10^{-6} Torr	0.02 Torr

The influence of substrate temperature was first examined for ZCO1R. In Fig. 4.1(a)-(d), it is evident that hysteresis were observed in all the films deposited under the same P_{O_2} irrespective of various substrate temperatures used. The curves shown in Fig. 4.1(a)-(d) are uncorrected. Since the diamagnetic contribution from the substrate is significantly larger than the ferromagnetic contribution from the film, the curves appear to be dominated by the diamagnetic signal from the substrates. In any case, it appears that the induced FM is not sensitive to the substrate temperature, at least in the temperature range of 400 -700 °C.

The second parameter, the cooling condition, was examined subsequently in our samples. Three films were grown at 500 °C and in an oxygen atmosphere of 10^{-1} Torr. Two were cooled down under P_{O_2} of 0.3 Torr and 0.02 Torr, respectively. Whereas the third one was cooled down rapidly under an oxygen atmosphere slightly above 760 Torr. As shown in the Fig. 4.2(a), the two films cooled down slowly to 100 °C under 0.3 Torr and 0.02 Torr in about 1 hour clearly exhibited room temperature (RT) FM, but the other did not exhibit detectable magnetic signal. Notice that the diamagnetic behavior is from the substrate.

Samples cooled down under 0.3 Torr and 0.02 Torr of oxygen pressures can be considered to be *in-situ* annealed for a certain period of time. Hong *et al.* [20] argued that perfect crystallinity doesn't go along with FM because they observed quite different lattice parameters in their ferromagnetic samples. Samples with mixed orientations as revealed by the XRD peaks of their samples shown in Fig. 4.3 were evident [20].

However, as shown in Fig. 4.2(b), the XRD patterns of our ZCO1R films display a nearly perfect *c*-axis orientation and with the FWHM of the (002) XRD line being less than 0.18° . Comparing results of [20], it appears that the crystallinity of the Cr-doped ZnO films does not play a significant role in giving rise to induced FM. It seems also to exclude the carried-mediated mechanism as the predominant physics in this system.

Alternatively, the cooling process can also be considered as a process that the oxygen “flowing in and out” of the samples. In this scenario, if the oxygen vacancies dominate the FM in ZCO1R films, the induced FM should be changed by tuning the oxygen pressure during growth. To check if this is indeed the case, we have investigated the magnetic properties for samples deposited at 500°C and cooled down to 100°C rapidly in about 25 minutes under 760 Torr of P_{O_2} while varying the oxygen pressure from 10^{-4} Torr to 10^{-1} Torr during growth. The results are shown in Fig. 4.4(a)-(d). It is obvious that the FM only appeared in samples with lowest oxygen pressure during growth. It is suggestive that the FM in ZCO1R films was dominated by the concentration of oxygen vacancies rather than the crystallinity of the films.

In ZnO, it is known that the transport properties are affected by the oxygen vacancies. Therefore, performing the resistivity measurement can illustrate how the oxygen vacancies varied in samples. However, because the sheet resistance of ZCO1R films was too large for us to measure (over $20\text{M}\Omega$), the indirectly alternative way is to measure the resistance of undoped ZnO samples grown under the same conditions.

The results of resistivity measurements are shown in table 4.2. The resistivity of samples deposited under lower oxygen pressure was smaller than that under higher oxygen pressure. However, after post-annealing, the sample, originally deposited at higher P_{O_2} and having larger resistivity, exhibits a dramatic reduction of resistivity from 18.9 Ω -cm to 0.3 Ω -cm. It implies that both the cooling process under low oxygen pressure and low growth oxygen pressure may have enhanced the formation of oxygen vacancies in the ZCO1R films, such that the FM is induced when the oxygen vacancies reach the donor polaron percolation threshold. It is consistent with the model that Coey *et al.* have proposed few years ago [12].



Table 4.2 Resistivity of ZnO films deposited at 500 °C

P_{O_2} (Torr)	Resistivity (Ω -cm)	Remarks
10^{-4}	1.93	None
10^{-1}	18.97	None
10^{-1}	0.31	Post-annealed under P_{O_2} of 0.3 Torr for 1 hour

Fig. 4.1(a)

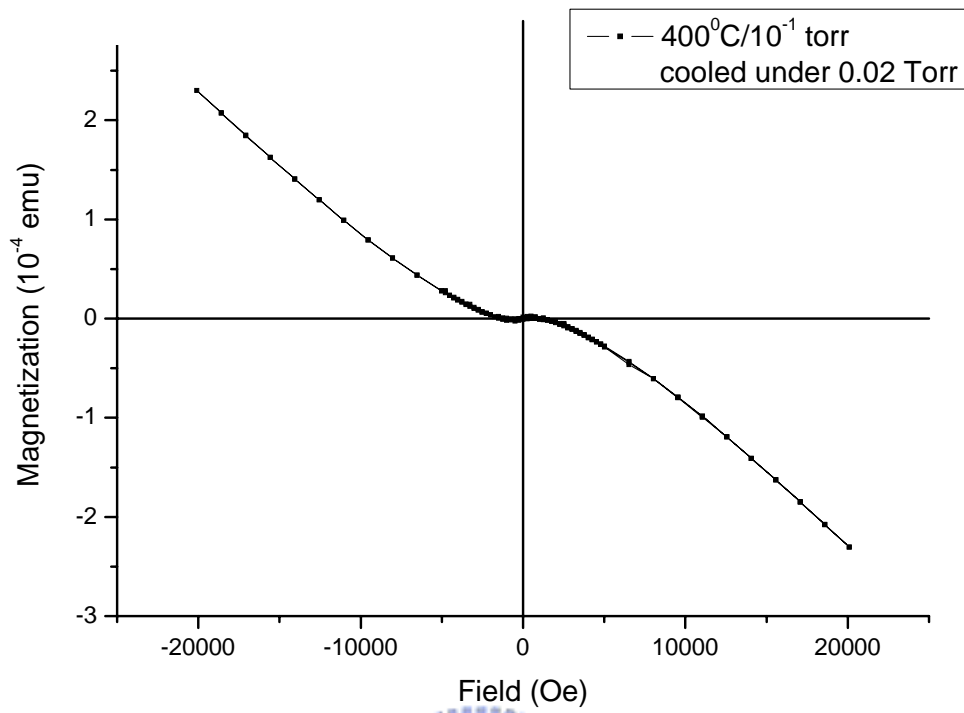


Fig. 4.1(b)

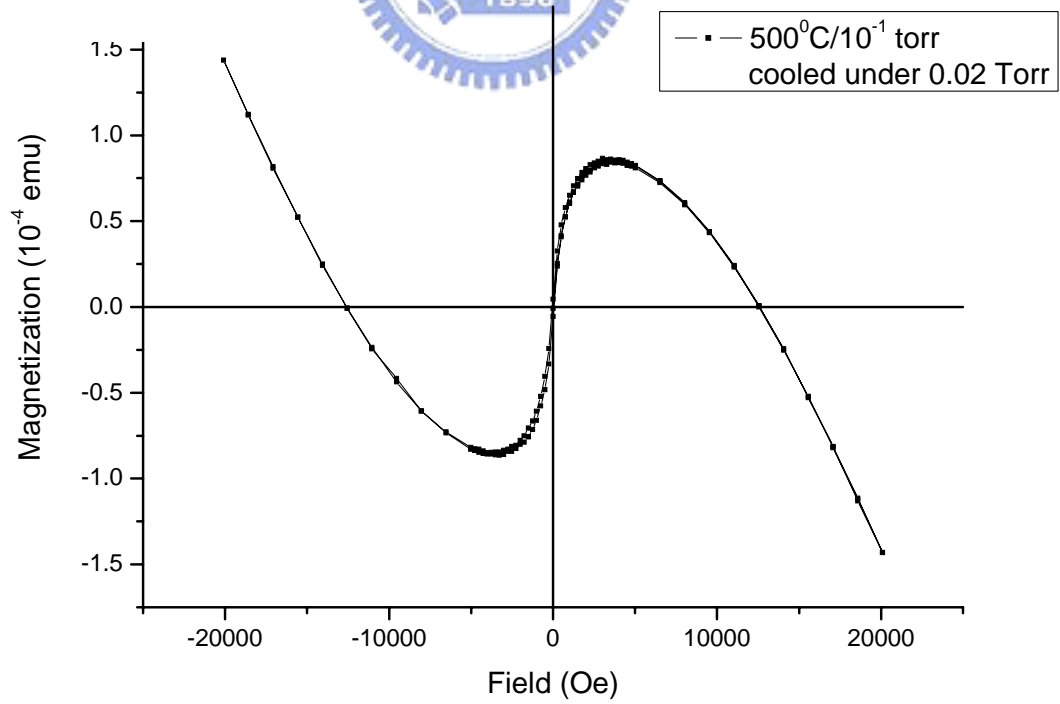


Fig. 4.1(c)

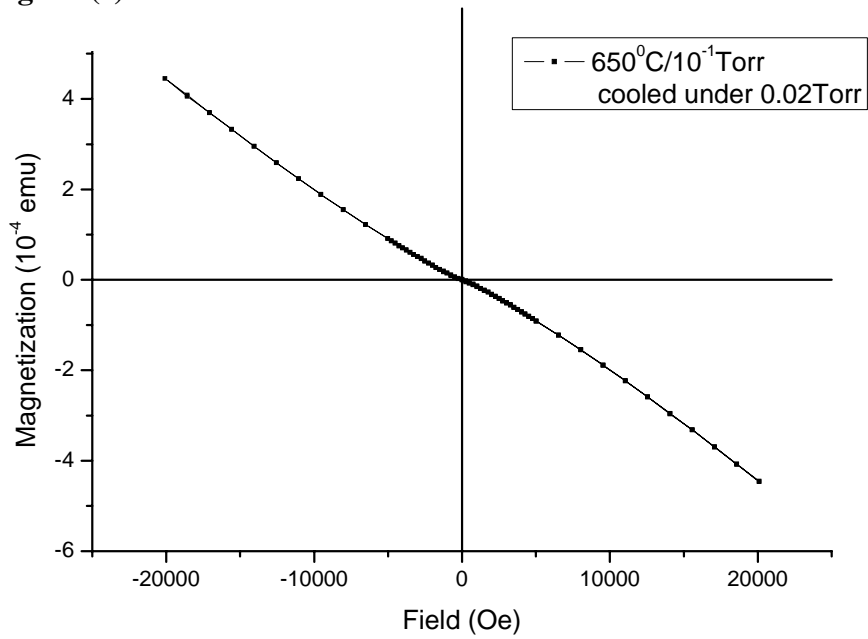


Fig. 4.1(d)

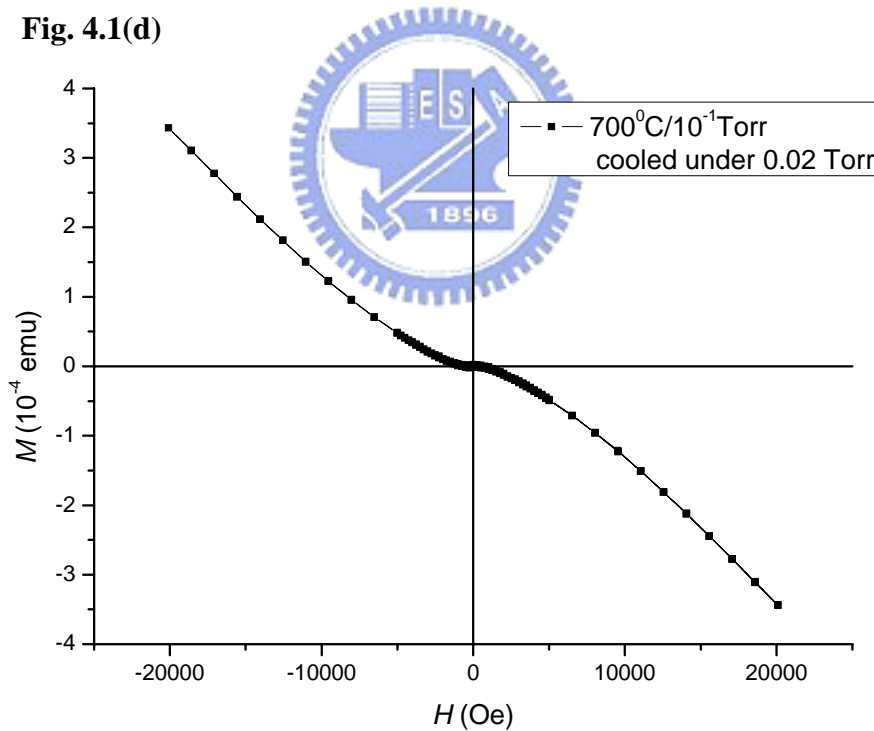


Fig. 4.1(a)-(d)

M - H curves for ZCO1R films fabricated at various substrate temperature under P_{O_2} of 0.1 Torr and cooled under P_{O_2} of 0.02 Torr.

The measurement was performed at 300 K, and the magnetic field was directed into the film surface perpendicularly (out-plane).

Fig. 4.2(a)

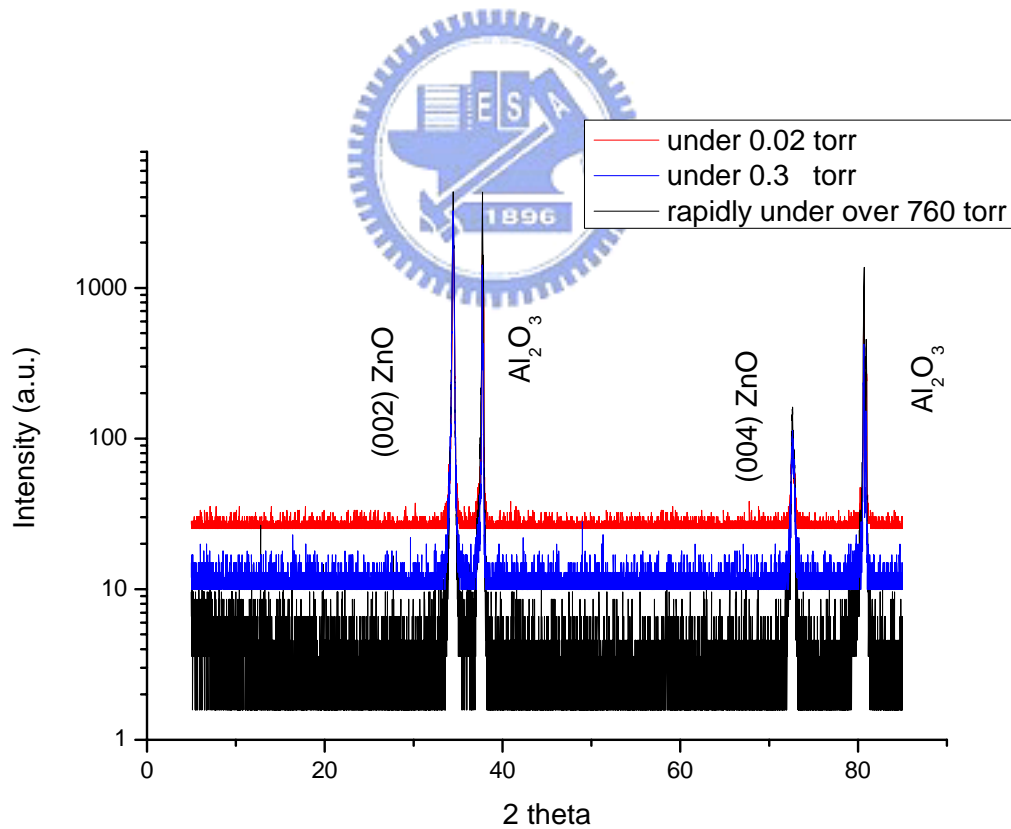
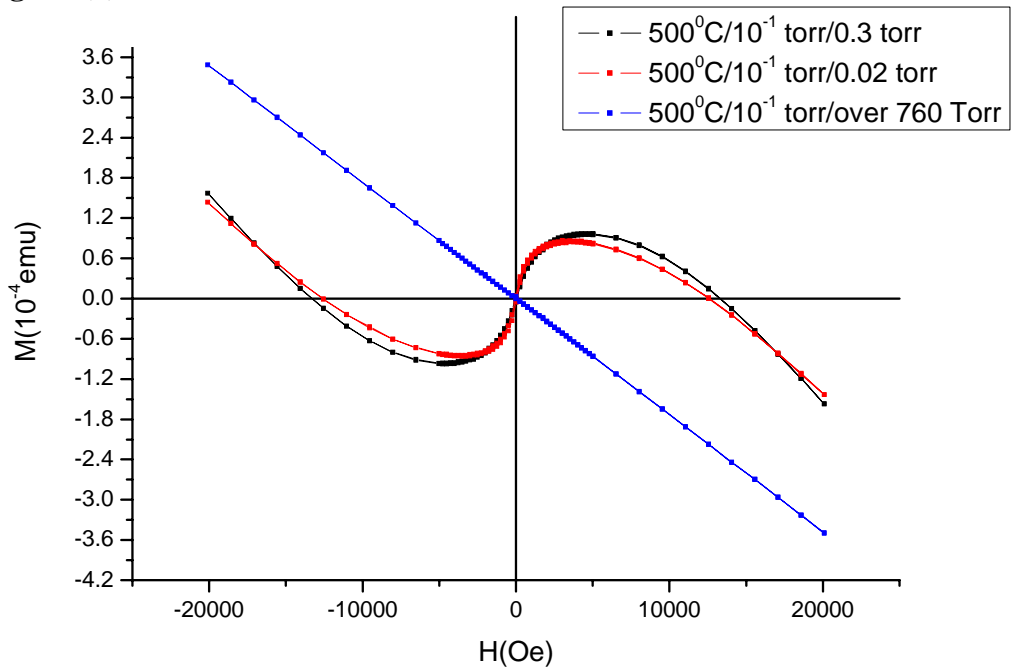


Fig. 4.2

ZCO1R films deposited at 500°C with P_{O_2} of 10^{-1} Torr and then cooled down under different oxygen pressure.

(a) M - H curves measured at 300 K with the out-plane applied field.

(b) XRD patterns for the samples shown in (a)

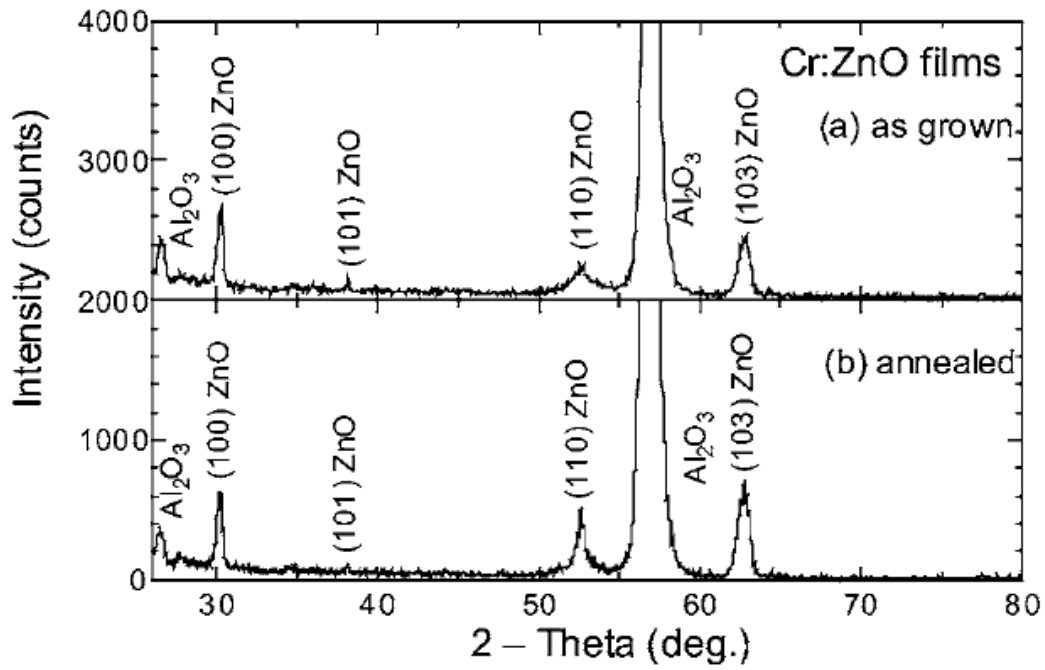


Fig. 4.3

XRD patterns for Cr:ZnO films fabricate at 650 °C under a P_{O_2} of 10^{-1} Torr: (a) as-grown film and (b) postannealed film. [19]

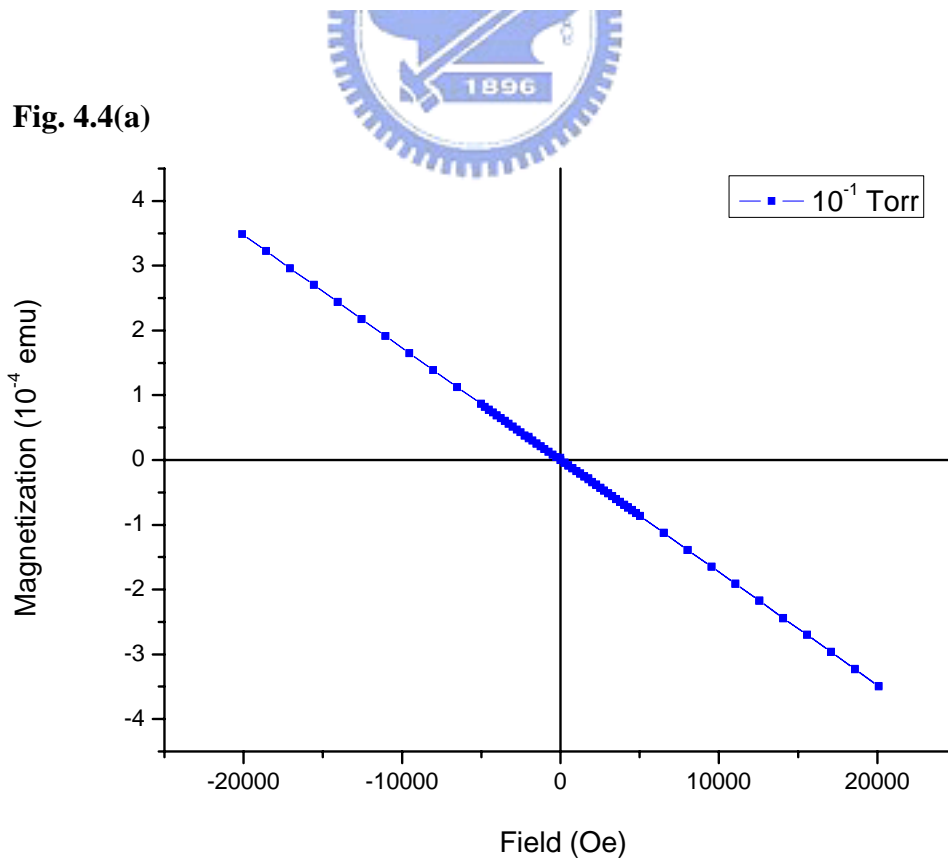


Fig. 4.4(a)

Fig. 4.4(b)

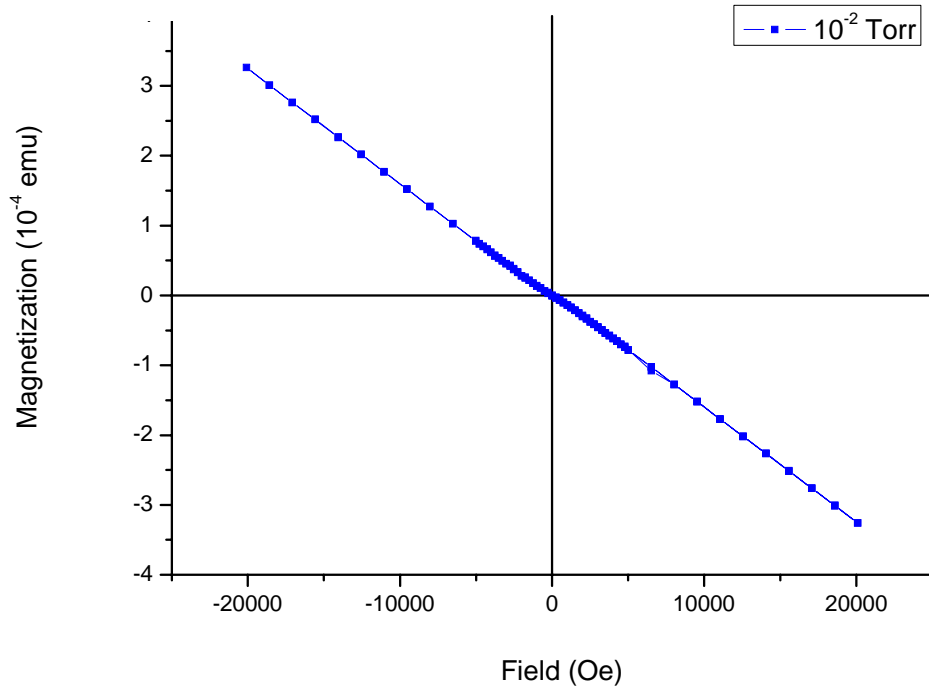


Fig. 4.4(c)

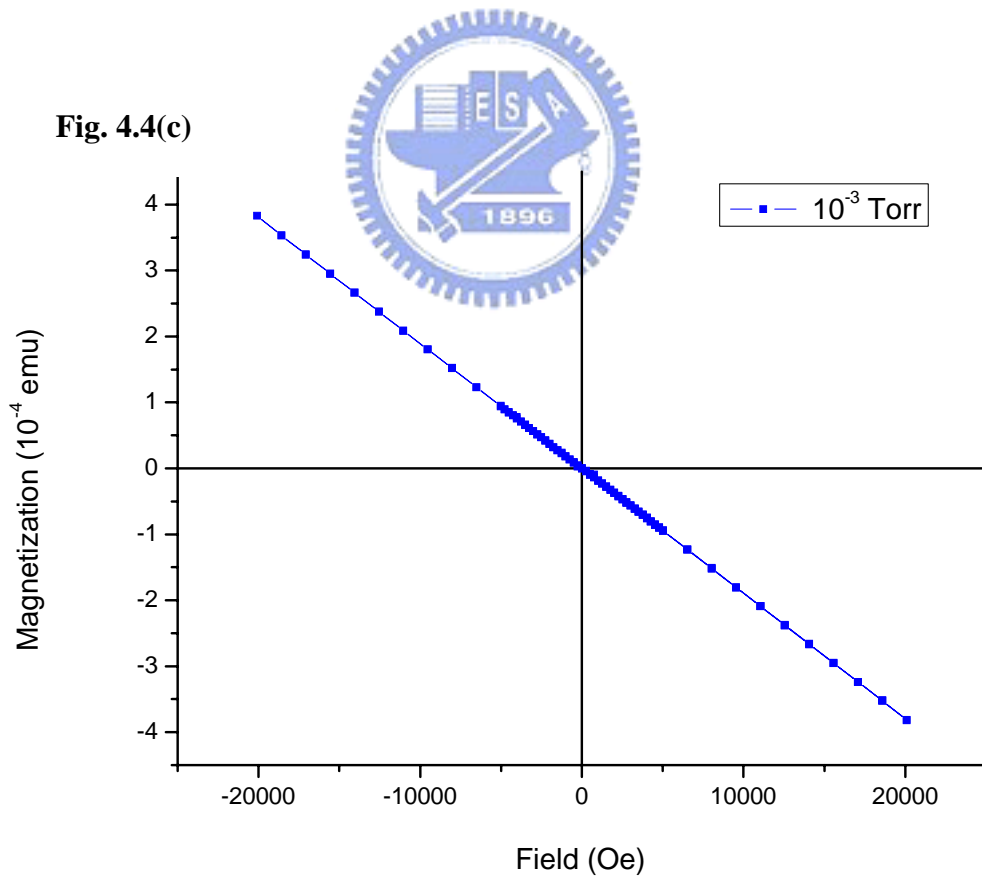


Fig. 4.4(d)

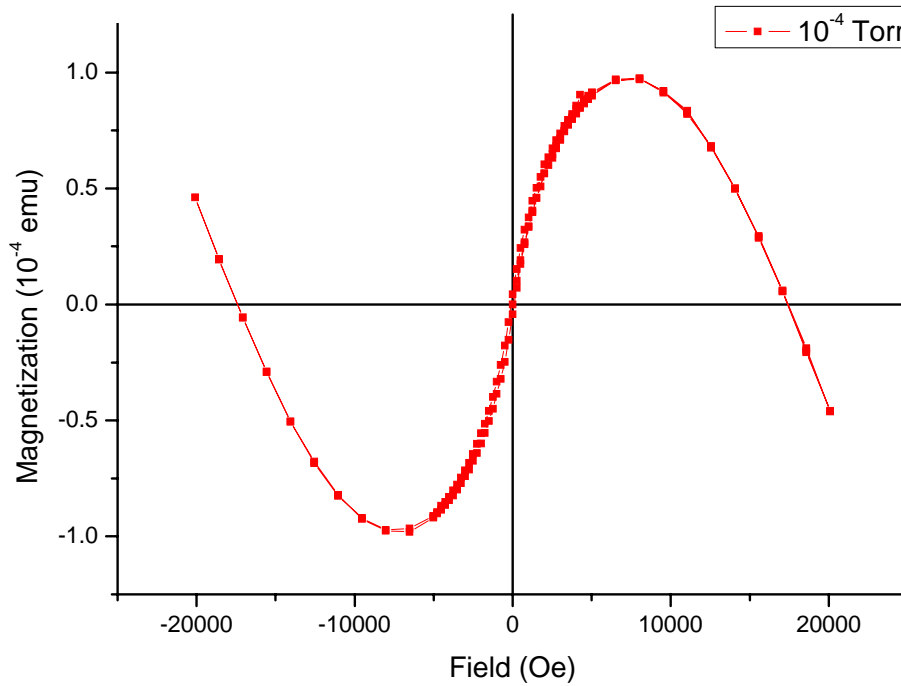


Fig. 4.4(e)

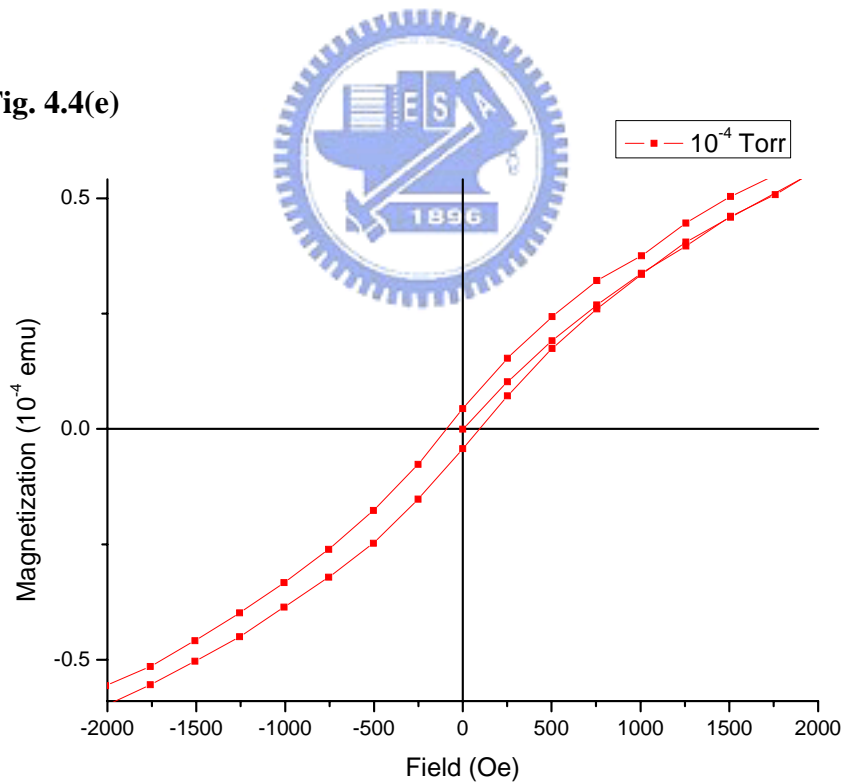


Fig. 4.4

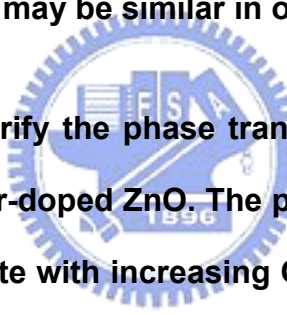
(a)-(d) ZCO1R films deposited at 500 $^{\circ}$ C under P_{O_2} of 10^{-1} , 10^{-2} , 10^{-3} , and 10^{-4} Torr respectively and then cooled under P_{O_2} over 760 Torr. All were measured at 300 K with out-plane H .

(e) shows the enlarged M - H curves of (d) from -2000 Oe to 2000 Oe

4.2 Phase transition from ferromagnetic spin-glass to ferromagnetic insulator

In order to further elaborate the underlying physics of the FM exhibited in the ZCO1R films, Fig. 4.5(a) shows the ferromagnetic in-plane $M-H$ curve of the ZCO1R film measured at 350 K and 5K. The sample was deposited at 500 °C with P_{O_2} of 10^{-4} Torr and then cooled down rapidly under 760 Torr of P_{O_2} . The temperature dependent magnetization of the ZCO1R film was also displayed in Fig. 4.5(b). The zero-field cooling (ZFC) (open symbols) and the field cooling (FC) (filled symbols) $M-T$ curves of this sample were measured at three different magnetic fields. The dissent between the ZFC and FC curves at a lower magnetic field demonstrates that the film could be in superparamagnetic state or become a spin-glass system. If the SPM was induced by ferromagnetic particles, such as Cr metal particles or ferromagnetic compounds, the magnetization should be increased as the doping concentration of Cr is increased [12]. Fig. 4.6(a) shows the in-plane $M-H$ curves of ZCO5R film measured at 350 K and 5K. The characteristic of FM, hysteresis, is obviously observed. The $M-T$ curves of this ZCO5R film measured at three different magnetic fields are shown in Fig. 4.6(b). The deposition parameters of this ZCO5R film were the same as that practiced for the sample shown in Fig. 4.5. By comparing these results, it is evident that the magnetization of ZCO5R film is reduced from 10.1 to $0.96 \mu_B/\text{Cr}$ as the Cr concentration is increased. It is believed that the

reduced magnetization could be resulted from the increased antiferromagnetic coupling between 3d ions as Cr concentration is raised. It is also consistent with Coey's prediction. Noted that the giant magnetic moment, $10.1 \mu_B/\text{Cr}$ larger than the spin-only moment, was observed in ZCO1 films. It might be attributed to the possibility that the orbital moment of Cr remains unquenched. In such case, an increase in the dopant concentration has been found to cause a rapid decrease in the moment (as observed in our sample) due to enhanced dopant-dopant associations leading to progressive orbital moment quenching. The decreased moment observed in our higher 5% Cr-doped samples suggest that the scenario may be similar in our case [8].



In this chapter we verify the phase transition proposed by Coey *et al.* [12] in the system of Cr-doped ZnO. The phase varies from spin-glass state to ferromagnetic state with increasing Cr concentration from 1% to 5%. The induced FM can be also controlled by tuning the oxygen vacancies in the film. Besides, the giant magnetic moment ($10.1 \mu_B/\text{Cr}$) observed in ZCO1 films may result from the unquenched Cr moment.

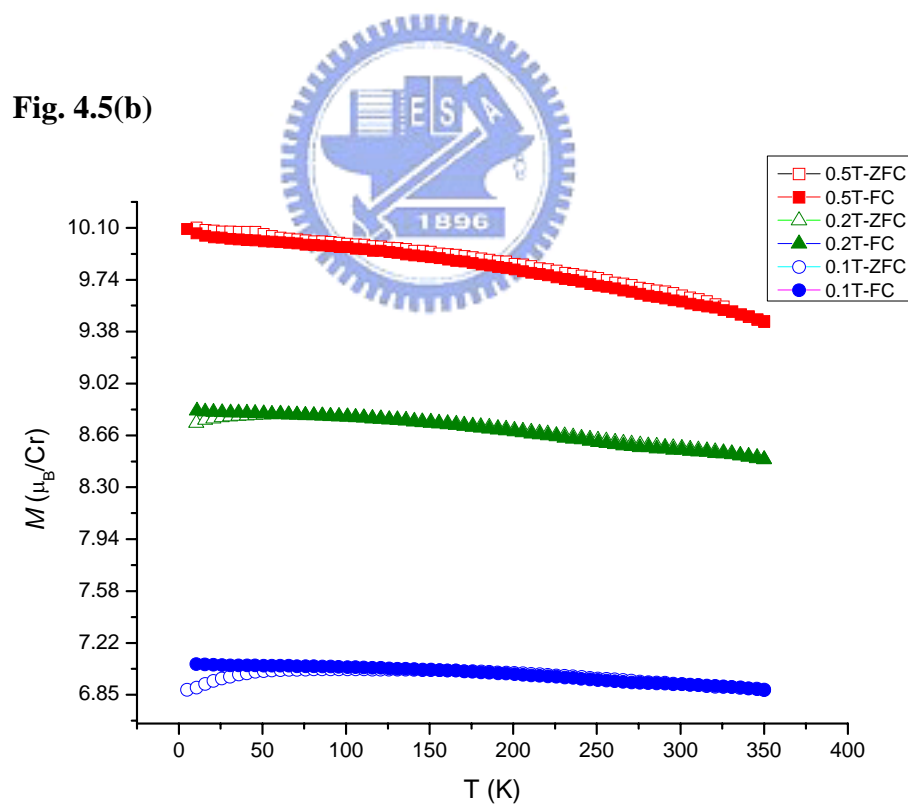
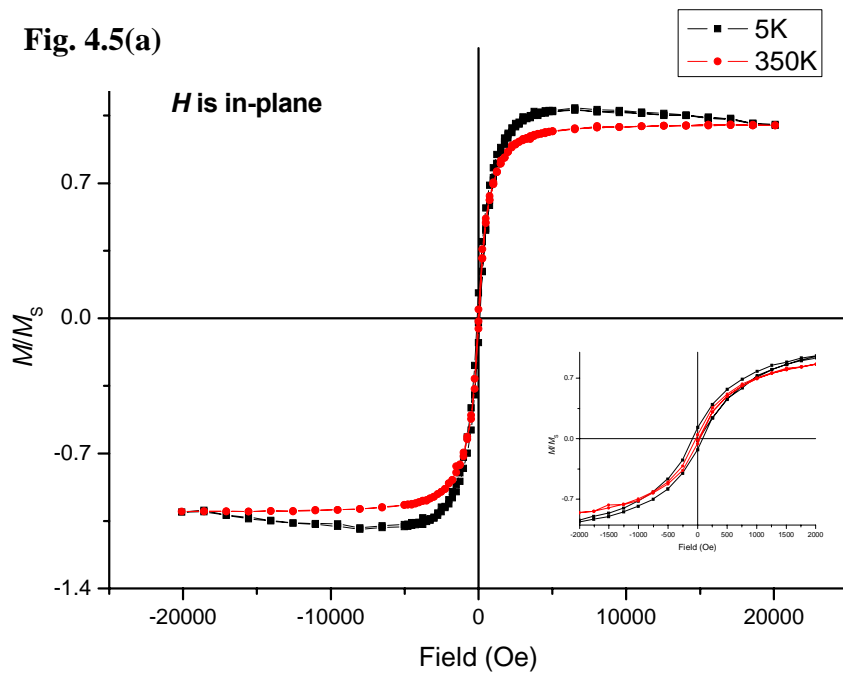


Fig. 4.5

Magnetic properties of ZCO1R film measured under in-plane applied field.

(a) Normalized M - H hysteresis curves at 350 K and 5 K.

(b) M - T curves at three different magnetic fields.

Fig. 4.6(a)

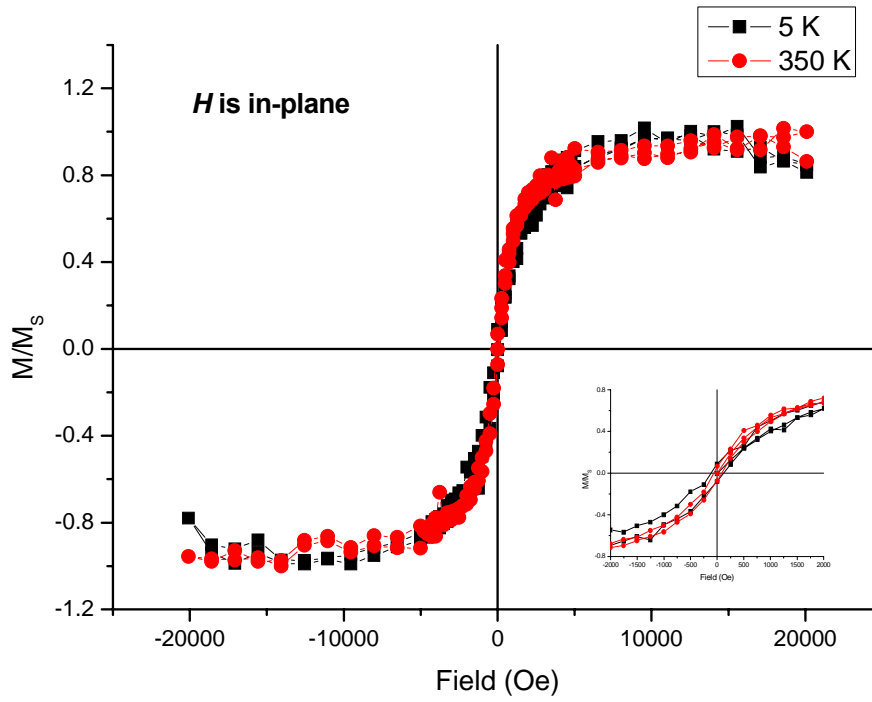


Fig. 4.6(b)

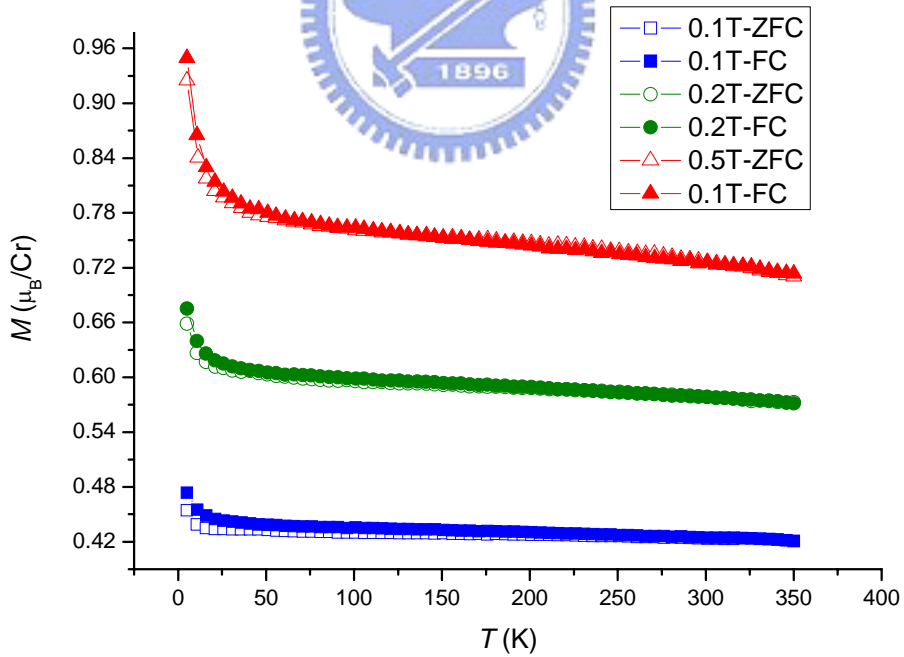


Fig. 4.6

Magnetic properties of ZCO5R film measured under in-plane applied field.

(a) Normalized M - H hysteresis curves at 350 K and 5 K.

(b) M - T curves at three different magnetic fields.

Chapter 5

Summary and conclusion

In this work, we have successfully fabricated ferromagnetic Cr-doped ZnO films with a nearly perfect c-axis orientation by PLD technique. Compared to Hong's work [19], the current results imply that the good crystallinity is not the primary factor for the induced FM in the system of Cr-doped ZnO. After performing systematic studies by treating each growth parameter separately, we find that the induced FM is insensitive to the substrate temperature, at least in the range of 400 °C to 700 °C. Furthermore, the induced FM is significantly dominated by the oxygen vacancies in the film. The concentration of oxygen vacancies can be tuned by the oxygen pressure not only during growth but also during the cooling process. It can be also used to explain the discrepancy between Robert's [17] and Hong's [19] work. Namely the different oxygen pressure during their post-annealed processes influenced the concentration of oxygen vacancies in their films and resulted in the different magnetic behaviors. We also find the phase transition from spin-glass state to ferromagnetic state with the increasing Cr concentration from 1% to 5 %. The observed magnetization is reduced as the Cr concentration is increased. It could result from the antiferromagnetic coupling between the Cr ions belonging to different magnetic bound polarons. The above observations are also consistent with Coey's prediction [12]. We also observed the giant magnetic

moment ($\sim 10.1 \mu_B/\text{Cr}$) in ZCO1 films. It might be attributed to the possibility that the orbital moment of Cr remains unquenched.



Reference

- [1] S. A. Wolf, D. D. Awschalom, R. A. Buhrman, J. M. Daughton, S. von Molnar, M. L. Roukes, A. Y. Chtchelkanova, D. M. Treger, *Science* **294**, 1488 (2001).
- [2] C. Zener, *Physical Review* **81**, 440 (1950).
- [3] T. Dietl, H. Ohno, F. Matsukura, J. Cibert, D. Ferrand, *Science* **287**, 1019 (2000).
- [4] Ü. Özgür, Ya. I. Alivov, C. Liu, A. Teke, M. A. Reshchikov, S. Doğan, V. Avrutin, S.J. Cho, and H. Morkoç, *Journal of Applied Physics* **98**, 041301 (2005).
- [5] S. J. Pearton, W. H. Heo, M. Ivill, D. P. Norton, and T. Steiner, *Semiconductors Science And Technology* **19**, R59 (2004).
- [6] P. Sharma, A. Gupta, K.V. Rao, F. J. Owens, R. Sharma, R. Ahuja, J. M. Osorio Guillen, B. Johansson, and G. A. Gehring, *Nature Materials* **2**, 673 (2003).
- [7] M. L. Reed, N. A. Elmasry, H. H. Stadelmaier, M. E. Ritums, M. J. Reed, C. A. Parker, J. C. Roberts and S. M. Bedair, *Applied Physics Letters* **79**, 3473 (2001).
- [8] S. B. Ogale, R. J. Choudhary, J. P. Buban, S. E. Lofland, S. R. Shinde, S. N. Kale, V. N. Kulkarni, J. Higgins, C. Lanci, J. R. Simpson, N. D. Browning, S. D. Sarma, H. D. Drew, R. L. Greene, and T. Venkatesan, *Physical Review Letters* **91**, 077205 (2003).
- [9] S. A. Chambers and S. Thevuthasan, R. F. C. Farrow, R. F. Marks, J. U. Thiele, L. Folks, M. G. Samant, A. J. Kellock, N. Ruzycki, D. L. Ederer, and U. Diebold, *Applied Physics Letters* **79**, 3467 (2001).

- [10] S. G. Yang, T. Li, B. X. Gu, Y. W. Du, H. Y. Sung, S. T. Hung, C. Y. Wong, and A. B. Pakhomov, *Applied Physics Letters* 83, 3746 (2003).
- [11] J. M. D. Coey, A. P. Douvalis, C. B. Fitzgerald, and M. Venkatesan, *Applied Physics Letters* 84, 1332 (2004).
- [12] J. M. D. Coey, M. Venkatesan, and C. B. Fitzgerald, *Nature Materials* 4, 173 (2005).
- [13] P. A. Stampe, R. J. Kennedy, Yan Xin, and J. S. Parker, *Journal of Applied Physics* 92, 7114 (2002).
- [14] C. Liu, F. Yun, B. Xiao, S. J. Cho, Y. T. Moon, H. Morkoç, Morad Abouzaid, R. Ruterana, K. M. Yu, and W. Walukiewicz, *Journal of Applied Physics* 97, 126107 (2005).
- [15] S. Dhar, O. Brandt, A. Trampert, L. Daweritz, K. J. Friedland, K. H. Ploog, J. Keller, B. Beschoten, and G. Güntherodt, *Applied Physics Letters* 82, 2077 (2003).
- [16] K. Sato and H. Katayama-Yoshida, *Semiconductors Science And Technology* 17, 367 (2002).
- [17] B. K. Roberts, A. B. Pakhomov, V. Shutthanandan, and K. M. Krishnana, *Journal of Applied Physics* 97, 10D310 (2005).
- [18] K. Ueda, H. Tabata, and T. Kawai, *Applied Physics Letters* 79, 988 (2001).
- [19] I. Satoh and T. Kobayashi, *Applied Surface Science* 216, 603 (2003).
- [20] N. H. Hong, J. Sakai, N. T. Huong, N. Poirot, and A. Ruyter, *Physical Review B* 72, 045336 (2005).
- [21] C. Kittel, *Introduction to Solid State Physics* (1996).
- [22] S. Nagata, P. H. Keesom, and H. R. Harrison, *Physical Review B* 19, 1633 (1979).

- [23] J. L. Dormann and D. Fiorani, **Magnetic properties of fine particles (1992).**
- [24] C. P. Bean and J. D. Livingston, **Journal of Applied Physics 30, 120S-129S (1959).**
- [25] S. Ramachandran, Ashutosh Tiwari, and J. Narayan, **Applied Physics Letters 84, 5255 (2004).**
- [26] L. J. van der Pauw, **Philips Technical Review 20, 220 (1958/59).**
- [27] <http://www.eeel.nist.gov/812/intr.htm>

